Next Energy 4 (2024) 100130

Contents lists available at ScienceDirect

Next Energy

journal homepage: www.sciencedirect.com/journal/next-energy

Research Article

Phase-field determination of NaSICON materials in the quaternary system Na_2O-P_2O_5-SiO_2-ZrO_2: II. Glass-ceramics and the phantom of excessive vacancy formation

Enkhtsetseg Dashjav[a], Marie-Theres Gerhards[a], Felix Klein[a,b], Daniel Grüner[c], Thomas C. Hansen[d], Jochen Rohrer[e], Karsten Albe[e], Dina Fattakhova-Rohlfing[a,b,f], Frank Tietz[a,f,*]

[a] Forschungszentrum Jülich GmbH, Institute of Energy and Climate Research, Materials Synthesis and Processing (IEK-1), Jülich D-52425, Germany
[b] University of Duisburg-Essen, Faculty of Engineering and Center for Nanointegration Duisburg-Essen (CENIDE), Lotharstraße 1, Duisburg 47057, Germany
[c] Forschungszentrum Jülich GmbH, Institute of Energy and Climate Research, Microstructure and Properties of Materials (IEK-2), Jülich D-52425, Germany
[d] Institut Max von Laue-Paul Langevin, 71 av. des Martyrs, CS 20156, Grenoble Cedex 9 38042, France
[e] Technical University of Darmstadt, Materials Modelling Division, Otto-Berndt-Straße 3, Darmstadt D-64287, Germany
[f] Forschungszentrum Jülich GmbH, Institute of Energy and Climate Research, Helmholtz Institute Münster: Ionics in Energy Storage (IEK-12), Jülich D-52425, Germany

ARTICLE INFO

Keywords:
NaSICON
Ionic conductivity
Solid electrolyte
Sodium
Quaternary phase diagram

ABSTRACT

This work focuses on a very narrow region in the quaternary system Na_2O-P_2O_5-SiO_2-ZrO_2 to explore the occasionally proposed deficiency in zirconium and oxygen content of Na^+ super-ionic conductor (NaSICON) materials. In addition, this region is known for the formation of glass-ceramics, but a systematic study of such materials has not been carried out yet. For this purpose, 2 series of compositions were defined and synthesized: $Na_{3.4}Zr_{2\text{-}3x/4}Si_{2.4\text{-}x/4}P_{0.6+x/4}O_{12\text{-}11x/8}$ and $Na_{3.4}Zr_{2\text{-}3x/4}Si_{2.4+x/4}P_{0.6+1.5x/4}O_{12\text{-}x/16}$. They only differ in the silicate and phosphate content. In the first series the molar content is constant, $n_{Si} + n_P = 3$. The latter series allows an excess of the 2 cations to meet the composition $Na_{3.1}Zr_{1.55}Si_{2.3}P_{0.7}O_{11}$ or alternatively re-written as $Na_{3.4}Zr_{1.7}Si_{2.52}P_{0.77}O_{12}$, which was formerly regarded as a superior material to the frequently reported composition $Na_3Zr_2Si_2PO_{12}$.

Several characterization techniques were applied to better understand the relationships between phase formation, processing, and properties of the obtained glass ceramics in the context of the quasi-quaternary phase diagram. The investigations gave clear evidence that a glass phase is progressively formed with increasing x. Therefore, compounds with $x > 0.2$ have to be regarded as glass-ceramic composites. The resulting NaSICON materials revealed a very limited Zr deficiency with charge compensation by Na ions and a non-detectable amount of oxygen vacancies verified by neutron scattering and atomistic simulations.

Hence, this work is the first systematic investigation of pretended Zr-deficient NaSICON materials, which clearly show the chemistry of a 2-phase region. The 2 investigated series are directed toward a region that is orthogonal to the series $Na_3Zr_{3\text{-}y}Si_2P_yO_{11.5+y/2}$ reported in the first part of this series of publications.

1. Introduction

Since the electrolyte is an indispensable and central part of batteries, the investigation and optimization of suitable liquid and solid electrolyte materials are crucial for the development of alkali-ion batteries and solid-state batteries, respectively. In the case of Na^+-ion-conducting solid electrolytes, development has been dominated during recent decades by the β/β”-aluminas. Batteries with these electrolytes have already been commercialized. The total ionic conductivity of β/β”-alumina ceramics can reach up to 6×10^{-3} S cm^{-1} at room temperature [1,2]. At the same time, materials with kosnarite structure [3] that were originally called Na^+ super-ionic conductors (NaSICONs) [4,5] have also been widely studied, but have never found their way into industrial battery applications [6]. Although the NaSICONs have been well-known solid electrolytes since the 1970s, there has been only very limited technological interest in these materials. However, since

* Corresponding author at: Forschungszentrum Jülich GmbH, Institute of Energy and Climate Research, Materials Synthesis and Processing (IEK-1), Jülich D-52425, Germany.
E-mail address: f.tietz@fz-juelich.de (F. Tietz).

https://doi.org/10.1016/j.nxener.2024.100130
Received 6 March 2024; Received in revised form 5 April 2024; Accepted 17 April 2024

solid-state batteries have become an emerging energy storage option during the recent decade, also the NaSICONs have experienced a revival not only in the academic field. Recently, the solid solution $Na_{1+z}Zr_2Si_zP_{3-z}O_{12}$ was re-investigated, and an ionic conductivity of 5×10^{-3} S cm^{-1} was obtained for $Na_{3.4}Zr_2Si_{2.4}P_{0.6}O_{12}$ [7], making both types of materials, that is, the β/β”-aluminas and the NaSICONs, particularly suitable for the development of solid-state batteries today. Especially with NaSICON materials a wide variety of (all-, almost- or quasi-) solid-state batteries have been presented during the recent years, for example, [6,8–16]. With regard to component manufacturing, a good knowledge of the chemical properties of these materials is necessary in order to be able to produce separators of high quality. To this end, detailed basic research is still required.

In the following, a number of solid solutions and series are mentioned, for which separate parameters or variables are always used. Therefore, a compilation of the variables follows here with their intended use for the further reading of this work:

- *w* in $Na_{1+w}Zr_{2-w/3}Si_wP_{3-w}O_{12-2w/3}$ is a variable for the nominal substitution of P with Si and additional Na^+ ions for charge compensation AND simultaneous Zr vacancy formation with oxygen vacancy formation
- *x* in $Na_{3.4}Zr_{2-3x/4}Si_{2.4-x/4}P_{0.6+x/4}O_{12-11x/8}$ and $Na_{3.4}Zr_{2-3x/4}Si_{2.4+x/4}P_{0.6+1.5x/4}O_{12-x/16}$ stands for a compositional variable used for the materials investigated in this study
- *y* in $Na_3Zr_{3-y}Si_2P_yO_{11.5+y/2}$ is a variable for the nominal substitution of Zr with P and additional O^{2-} ions for charge compensation
- *z* in $Na_{1+z}Zr_2Si_zP_{3-z}O_{12}$ is a variable for the substitution of P with Si and additional Na ions for charge compensation
- *a* in $Na_{1+4a}Zr_{2-a}P_3O_{12}$ is a variable for Zr vacancy formation and charge compensation with additional Na^+ ions
- *b* and *c* in $Na_{3-b}Zr_{2-c}Si_2PO_{12-b/2-2c}$ give experimentally verified ranges of compositions
- *d* in $Na_5ZrSi_{3-d}P_dO_{10.5+d/2}$ gives an experimentally verified range of compositions
- *e* in $Na_3Zr_{2-e/4}Si_{2-e}P_{1+e}O_{12}$ is a variable for the substitution of Si with P and Zr vacancy formation for charge compensation
- *f* in $Na_{1+z}Zr_{2-f}Si_zP_{3-z}O_{12-2f}$ is a variable for Zr vacancy formation and charge compensation with additional oxygen vacancies, *z* has the same meaning as above
- *a, f, z* in $Na_{1+4a+z}Zr_{2-a-f}Si_zP_{3-z}O_{12-2f}$ appear in combination and have the same meaning as above
- *g* in $Na_{2+g}Si_{1-g}P_gO_{3+g}$ and $Na_{2+g}Si_{2-2g}P_gO_{5+3g}$ is the molar fraction of Na_3PO_4 in a mixture with Na_2SiO_3 and $Na_2Si_2O_5$, respectively.

In terms of materials science, to date, the series $Na_{1+z}Zr_2Si_zP_{3-z}O_{12}$ [4,5] has been extensively investigated due to the high ionic conductivity of the materials with $2 < z < 2.5$. In addition, its starting member, $NaZr_2P_3O_{12}$, also belongs to a series of ternary compositions that can be expressed in a general form as $Na_{1+4a}Zr_{2-a}P_3O_{12}$ with $0 < a < 1$ [5,17] and partial occupation of vacant Zr sites with Na^+ ions. Both series are shown in Fig. 1 as bold blue lines. However, the existence of NaSICON materials is not restricted to these 2 solid solutions. In the first part of our investigations within the Na_2O-P_2O_5-SiO_2-ZrO_2 system [18], the results of the series $Na_3Zr_{3-y}Si_2P_yO_{11.5+y/2}$ clearly revealed a single-phase region of monoclinic NaSICON materials from the nominal composition $Na_3Zr_{2.25}Si_2P_{0.75}O_{11.875}$ to $Na_3Zr_{1.67}Si_2P_{1.33}O_{12.17}$ with $Na_3Zr_2Si_2PO_{12}$ as an intermediate composition. The width of chemical variation suggests a limited flexibility of site occupancies of cations that are usually found on other crystallographic positions. This flexibility vanishes when the Zr/P ratio is further decreased. As a consequence, the compositions $Na_3Zr_{1.33}Si_2P_{1.67}O_{12.33}$ and $Na_3ZrSi_2P_2O_{12.5}$ decompose to 2 NaSICON phases, tentatively identified as $Na_{3-b}Zr_{2-c}Si_2PO_{12-b/2-2c}$ with $0.7 < c < 0.8$ and $0.1 < d < 0.2$ and as $Na_5ZrSi_{3-d}P_dO_{10.5+d/2}$ with $2.9 < e < 3$ crystallizing in $R\bar{3}c$ and *R32* symmetry, respectively [5,19]. These

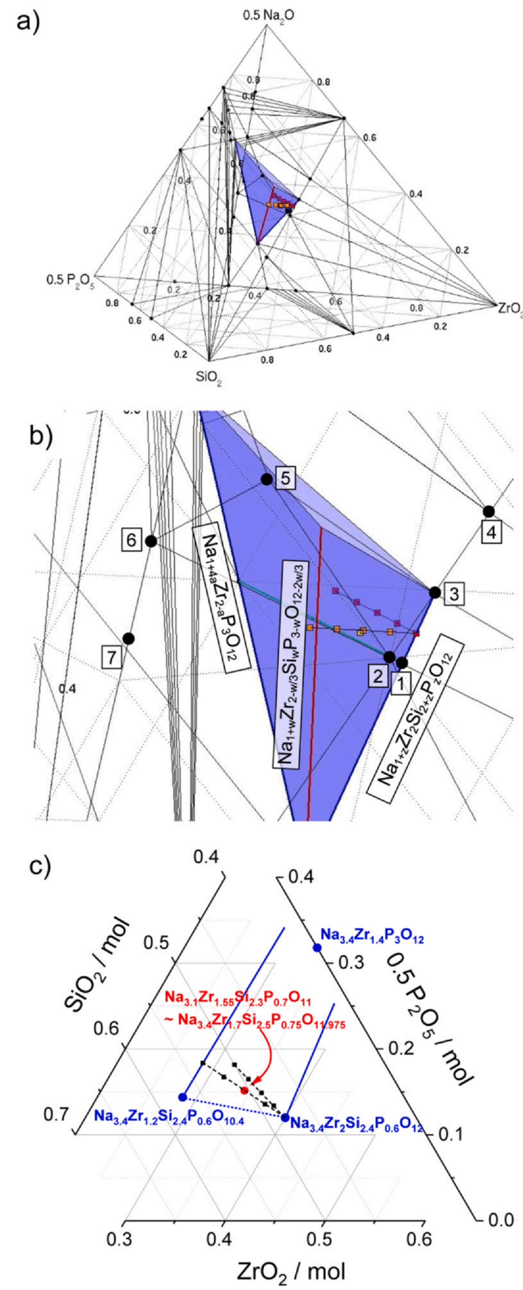

Fig. 1. **a)** The quaternary phase diagram Na_2O-SiO_2-ZrO_2-P_2O_5 visualizing the position of the nominal series $Na_{3.4}Zr_{2-3x/4}Si_{2.4-x/4}P_{0.6+x/4}O_{12-11x/8}$ (series 1, dark red squares) and $Na_{3.4}Zr_{2-3x/4}Si_{2.4+x/4}P_{0.6+1.5x/4}O_{12-x/16}$ (series 2, orange squares). The blue compressed tetrahedron corresponds to the potential phase field of NaSICON materials constructed on the basis of the 3 solid solutions shown as blue and red lines [26]. **b)** Enlarged view of Fig. 1a, also showing the position of $Na_{3.1}Zr_{1.55}Si_{2.3}P_{0.7}O_{11}$ [20] as a yellow square close to the middle orange square. For comparison, the large black circle (no. 1) corresponds to $Na_3Zr_2Si_2PO_{12}$, which is the starting point for series $Na_3Zr_{2-e/4}Si_{2-e}P_{1+e}O_{12}$ (dark green line) [27]. The other numbers from 2 to 7 belong to the compositions $Na_2ZrSi_2O_7$, $Na_4Zr_2Si_3O_{12}$, Na_2ZrSiO_5, $Na_{14}Zr_2Si_{10}O_{31}$, $Na_2Si_2O_5$, and $Na_2Si_3O_7$, respectively. **c)** Ternary isopleth plot of the relevant region in Fig. 1a. The blue lines indicate the cross-section of the blue NaSICON tetrahedron.

results show that NaSICON compositions exist, which are off-site of the series $Na_{1+z}Zr_2Si_zP_{3-z}O_{12}$ [4,5] and $Na_{1+4a}Zr_{2-a}P_3O_{12}$ [19].

The motivation for investigating the 2 series $Na_{3.4}Zr_{2-3x/4}Si_{2.4-x/4}P_{0.6+x/4}O_{12-11x/8}$ (series 1) and $Na_{3.4}Zr_{2-3x/4}Si_{2.4+x/4}P_{0.6+1.5x/4}O_{12-x/16}$ (series 2) is the work of von Alpen et al. [20] who reported high ionic conductivity in the compound $Na_{3.1}Zr_{1.55}Si_{2.3}P_{0.7}O_{11}$ and postulated the solid solution $Na_{1+w}Zr_{2-w/3}Si_wP_{3-w}O_{12-2w/3}$ (bold red line in Fig. 1). With this third solid solution, the blue distorted tetrahedron in Fig. 1 can be constructed to visualize the occurrence of the NaSICON phase in the quaternary phase diagram.

It should be noted that the composition mentioned above does not belong to this solid solution and no systematic investigation of this latter series has been carried out.

In subsequent publications, the 2-phase nature of the compound $Na_{3.1}Zr_{1.55}Si_{2.3}P_{0.7}O_{11}$ was elucidated and it was shown that a high amount of glass phase is present together with a crystalline NaSICON phase [21–25]. These 2 phases can easily be derived from the above stoichiometry by re-writing the chemical formula as $Na_4Zr_2Si_{2.97}P_{0.9}O_{14.19}$. This not only gives a nearly stoichiometric ratio of the cations, it also shows that there is too much sodium and silicon in the composition for a NaSICON material. More specifically, when the compositions $Na_{3.4}Zr_2Si_{2.4}P_{0.6}O_{12}$ or $Na_{3.1}Zr_2Si_{2.1}P_{0.9}O_{12}$ are subtracted from this formula, 0.3 mol $Na_2Si_2PO_{7.5}$ or $Na_2Si_2O_5$ remain as potential glass phases, respectively. Consequently, it was regarded as important to explore in more detail the impact of Zr deficiency in NaSICON materials and to identify the phase stability region in this area of the quaternary phase diagram. The starting point of this work is the composition $Na_{3.4}Zr_2Si_{2.4}P_{0.6}O_{12}$, possessing a very high total ionic conductivity of about 5×10^{-3} S cm^{-1} [7]. On the one hand, the stoichiometry was varied by increasing the Zr deficiency and maintaining the total amount of Si and P at 3 mol/formula unit ($Na_{3.4}Zr_{2-3x/4}Si_{2.4-x/4}P_{0.6+x/4}O_{12-11x/8}$; series 1) resulting in a large number of hypothetical oxygen vacancies. On the other hand, the Zr deficiency was increased in the same way, but an excess of Si and P was permitted ($Na_{3.4}Zr_{2-3x/4}Si_{2.4+x/4}P_{0.6+1.5x/4}O_{12-x/16}$; series 2) to meet the "von Alpen composition" at x = 0.4. Fig. 1 illustrates the compositional variation in the quaternary phase diagram. In Fig. 1c, the compositional variation is shown in a simplified ternary diagram. The blue lines indicate the cross-section through the blue NaSICON tetrahedron (Fig. 1a and 1b) [26] at the molar fraction ξ_{Na} = 0.405. The investigated series are shown as black dotted lines. It should be noted that the simplification of this isopleth representation is not fully precise due to slightly varying ξ_{Na} values: for series 1 and series 2 from 0.405 to 0.436 and 0.410, respectively, that is, the lines gradually deviate from the image plane. In this work, the 2 series are characterized by thermal analysis, sintering experiments, and diffraction methods to better understand the chemical properties and to obtain more precise insight into the blue region shown in Fig. 1. In a forthcoming paper, we will report on the physical properties of the materials including ionic and thermal conductivity.

2. Experimental

Different powders within the 2 series with x = 0, 0.2, 0.4, 0.6, and 0.8 were synthesized by the solution-assisted solid-state reaction, as described elsewhere [28,29]. More information about precursors, their ratios, and the error range of the compositions is described in the Supplementary information (Table S1). The dried solid mixtures were annealed in an oven at 800 °C for 3 h to form an amorphous raw powder. After this heat treatment gaseous species (H_2O, NO_2, CO_2) were then removed and the primary particles of the powder displayed a nearly spherical shape with a diameter of < 50 nm [29]. The calcined powders were then ball-milled in ethanol with zirconia balls on a roller bench for 4 days. After drying, the powders were used either as prepared to this stage or sintered at 1250 °C for 4 h to get an isothermal state of the different compositions.

Differential thermal analysis and thermogravimetry (DTA/TG) measurements were carried out on the calcined powders up to 1600 °C with heating and cooling rates of 300 K/h. In addition, differential scanning calorimetry/thermogravimetry (DSC/TG) measurements were performed on the sintered powders in the air up to 1400 °C (in some cases up to 1425 °C) with heating and cooling rates of 600 K/h. The samples were kept at the maximum temperature for 0.5 h to evaluate the evaporation rate of Na_2O [18]. For both sets of measurements, the simultaneous thermal analyzer STA449F1 Jupiter from NETZSCH-Gerätebau GmbH was used. Dilatometry experiments were performed with a 402C dilatometer (also from NETZSCH-Gerätebau GmbH) applying a heating rate of 300 K/h. During the measurements, the shrinkage was recorded until a value of 25% was reached as an end-of-measurement criterion to avoid the melting of the samples.

For sintering experiments in a chamber furnace, the powders were pressed into pellets (diameter = 13 mm, thickness ~2 mm) applying a pressure of about 90 MPa followed by sintering for 4 h on Pt foil. The sintering temperatures were varied in steps of 20 K from 1010 °C to 1250 °C. At maximum temperature, the samples were exposed to a dwell time of 4 h. After sintering, the experimental density was obtained using the weight and volume of the pellets. To calculate the relative density, the theoretical density of $Na_{3.4}Zr_2Si_{2.4}P_{0.6}O_{12}$ (3.303 g cm^{-3}) [7] was used. Since a substantial amount of glass phase was observed with increasing x, the theoretical density was corrected with the volume fraction and density of the glass phase. Here, it was assumed that $Na_2Si_2O_5$ is the dominant glass composition, which has a density of 2.363 g cm^{-3}. This value is lower than crystalline $Na_2Si_2O_5$ (α-$Na_2Si_2O_5$: 2.48 g cm^{-3} [30], 2.50 g cm^{-3} [31], β-$Na_2Si_2O_5$: 2.62 g cm^{-3} [32]), or $Na_3Si_2PO_8$ (2.79 g cm^{-3}), which might also be regarded as possible glass composition [33]. As a glass, $Na_3Si_2PO_8$ has a similar density of 2.418 g cm^{-3}. This scatter of density of the secondary phase increases the error in determining the relative density of the sintered specimens, but it does not change the observed general trends.

The specimens sintered at 1250 °C were characterized with respect to their crystal structure and phase purity using X-ray diffraction (XRD) measurements from 2θ = 10° to 139° with a step size of 0.02° and a scan time of 0.75 s/step. The measurements were recorded with a Bruker D4 Endeavor diffractometer using Cu K_a radiation. The Rietveld refinements of the collected XRD data were performed using the software Jana2006 [34].

The neutron diffraction (ND) study was performed on powders at the high-flux 2-axis D20 beam line at the Institut Laue-Langevin (Grenoble, France). A take-off angle of 118° from the Ge(117) monochromator (λ ~ 1.3581 Å) was chosen and each measurement was carried out for 45 minutes at 295 K with position-sensitive detectors spanning from 2° to 160° angular range with steps of 0.1°. Vanadium cylinders of 5 mm in diameter were filled with powder of 8 NZSP samples (~1.2 g each). The Rietveld refinements were carried out using the Thompson-Cox-Hastings pseudo-Voigt peak shape function, implemented in the software package Fullprof Suite [35,36]. The diffraction background was interpolated between manually set points. Lattice parameters, zero-point shifts, and peak shapes were initially refined using the Le Bail method. During the final cycles of the refinement, the occupancy factors for mixed occupied Si/P sites were constrained to add up to full occupation. Their thermal displacement and position parameters were constrained to be equal. The thermal displacement parameters and site occupation factors (SOF) of Na, Si/P atoms were refined in alternating cycles until convergence was reached (< 0.1% difference between cycles) and fixed at the last cycle to result in a final stoichiometry.

The microstructural characterization was performed on polished cross-sections of samples prepared by standard metallographic procedures using water-free lubricants and polishing media. The microstructure was investigated in a MERLIN field emission scanning electron microscope (FE-SEM, Carl Zeiss) with an accelerating voltage of 10 kV. Quantitative image analysis was carried out with Olympus Stream software. Energy-dispersive X-ray (EDX) spectra were acquired using an X-max 80 detector (Oxford Instruments). For quantitative analysis of the EDX spectra (AZtec software, Oxford Instruments), $Ca_3(PO_4)_2$ was used as the standard for P and $ZrSiO_4$ was used as the standard for O, Si, and Zr. The Na content was calculated from the contents of Si, P, and Zr.

Atomistic simulations were performed using the large-scale atomic/molecular massively parallel simulator (LAMMPS) [37]. As an interaction

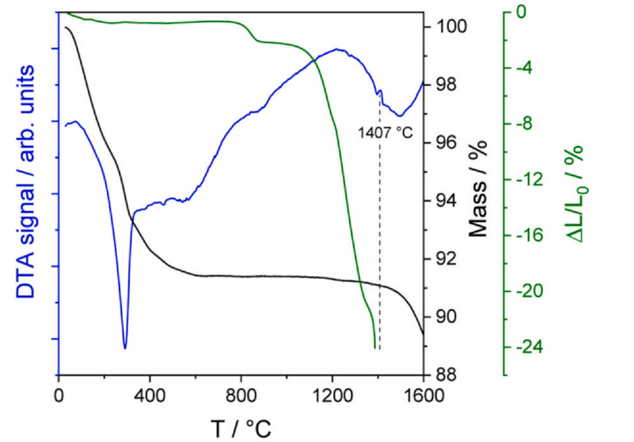

Fig. 2. Exemplary DTA/TG measurement of $Na_{3.4}Zr_2Si_{2.4}P_{0.6}O_{12}$ combined with the dilatometric shrinkage curve indicating the consistent melting point at 1407 °C.

model, a machine-learning potential (MLP) [38] based on the atomic cluster expansion (ACE) framework [39–41] has been trained on a large dataset of unaries, binaries, ternaries, quaternaries and quinaries in the chemical space of Na-Zr-P-Si-O. The training energies and forces were calculated using density functional theory as implemented in the real-space grid-based projector-augmented wave code [42,43]; for exchange and correlation, the van-der-Waals-CX-13 functional was used [44]. A brief validation of the NaSICON ACE MLP for the present context is given in the Supplementary Information section. Further details and an in-depth presentation of the underlying data, fitting procedure, and further tests will be published elsewhere.

3. Results and discussion

3.1. Thermal analysis

DTA/TG measurements showed an initial weight loss between 8 wt% and 20 wt% up to 600 °C due to remaining water and carbonates after the synthesis. The weight loss coincides with exothermic signals in the DTA curve. A representative measurement is shown for the composition $Na_{3.4}Zr_2Si_{2.4}P_{0.6}O_{12}$ in Fig. 2. Most of the measurements did not show any further DTA characteristic features. In some cases, as shown in Fig. 2, a small endothermic peak is visible at high temperatures. This is related to the melting point of the material and coincides very well with the endpoint of the dilatometric sintering curve. An additional weight loss, starting at about 1300 °C and exponentially increasing with increasing temperature, is associated with the evaporation of Na_2O [18].

After sintering and phase formation, DSC/TG measurements clearly revealed 3 caloric signals: a melting point at low temperatures of 1057 ± 12 °C, a melting point at high temperature related to the NaSICON phase, and the solidification temperature of the mixture during cooling. The peak temperatures of the 3 events are summarized in Fig. 3 for both series. For the starting composition $Na_{3.4}Zr_2Si_{2.4}P_{0.6}O_{12}$ (x = 0) and the first member of series 1 with x = 0.2, $Na_{3.4}Zr_{1.85}Si_{2.35}P_{0.65}O_{11.73}$, the melting point at low temperature could not be detected, but for the other samples the signal increases with x. Therefore, it is assigned to the expected increasing amount of a glass phase. For series 1, the melting point of the glass phase slightly increases from 1062 °C to

1069 °C, whereas it tentatively decreases from 1055 °C to 1044 °C for series 2. In general, the melting point of the crystalline NaSICON phase decreases with increasing x in both series. However, in series 1, the sample with x = 0.4 deviates from the general trend and shows a peak temperature at 1420 °C, before the values decrease to 1380 °C for x = 0.8. In series 2, there is a continuous decrease down to 1350 °C.

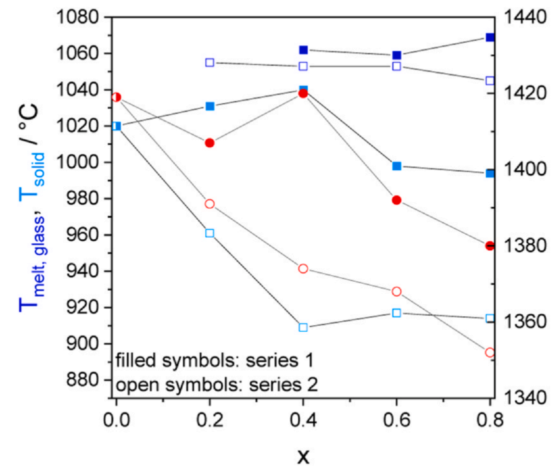

Fig. 3. Melting and solidification temperatures for the compositions in series 1 and series 2. The dark blue, light blue, and red symbols correspond to the melting points of the glass phase, the solidification temperatures during cooling, and the melting points of the crystalline phase, respectively.

Taking the liquidus line and the melting points of the series $Na_{1+z}Zr_2Si_{2+z}P_{1-z}O_{12}$ [45] as a calibration curve, the variation of the measured melting points between 1350 °C and 1420 °C would then correspond to compositions between z = 2.26 and z = 2.43, respectively. The resulting sodium content of the specimens is listed in Table 1.

The solidification temperatures vary between 994 °C and 1040 °C for series 1 and between 904 °C and 1020 °C for series 2 (Fig. 3). The measured solidification temperatures do not reflect the solidification of the glass phase, because the NaSICON phase also melted and decomposed. Therefore, the composition of the molten materials is different than the glass phase during heating. These temperatures are not further considered here but might be of interest if NaSICON materials are to be prepared via the melt-quenching method.

3.2. Dilatometry

The shrinkage behavior of the pressed pellets made of calcined powders was recorded with dilatometry to identify the optimal sintering temperature. Only the samples with the composition $Na_{3.4}Zr_2Si_{2.4}P_{0.6}O_{12}$ (x = 0) and $Na_{3.4}Zr_{1.85}Si_{2.35}P_{0.65}O_{11.73}$ (series 1, x = 0.2) show an ordinary shrinkage curve (Fig. 4) as known for ceramic materials. From the 2 curves reasonable sintering temperatures can be deduced in the region where the shrinkage is 15–20%.

For the other samples, a multiple step shrinkage behavior was observed, which is associated with an increasing amount of amorphous material. It is worth noting that the strongest shrinkage at reduced temperatures was observed for samples with x = 0.4 in both series. The appearance of glassy phases can be identified by the shrinkage steps at about 850 °C and 1150 °C for series 1 and at about 850 °C and 1050–1150 °C for series 2, always followed by an interval without shrinkage. In these cases, the shrinkage curves suggest a partial melting and recrystallization of the samples [18]. The extent of the shrinkage is misleading because the partial melting can cause a gliding of crystalline particles due to the low pressure of the pushrod of the dilatometer. Therefore, the length change is at least partially induced by plastic deformation, which is also visible in all curves at high temperatures and beyond a shrinkage of 20% and at about 850 °C and 1050–1150 °C for series 2, always followed by an interval without shrinkage. In these cases, the shrinkage curves suggest a partial melting and recrystallization of the samples [18]. The extent of the shrinkage is misleading because the partial melting can cause a gliding of crystalline particles due to the low pressure of the pushrod of the dilatometer. Therefore, the length change is at least partially induced by plastic deformation,

Table 1
Sodium contents (in mol per formula unit) according to the formula $Na_{1+z}Zr_2Si_{2+z}P_{1-z}O_{12}$ derived from DSC and XRD measurements and to the formula $Na_{1+z+4a}Zr_{2-a}Si_{2+z}P_{1-z}O_{12}$ derived from ND and EDX measurements.

Series	x	Na content from DSC	Na content from XRD	Na content from ND	Na content from EDX
1 + 2	0	3.50	3.59	3.62	3.80
1	0.2	3.46	3.37	3.56	3.80
1	0.4	3.50	3.42	3.58	3.83
1	0.6	3.40	3.26	3.47	3.86
1	0.8	3.36	3.39	3.47	3.87
2	0.2	3.40	3.36	3.47	3.65
2	0.4	3.34	3.42	3.44	3.81
2	0.6	3.33	3.50	n.a.	3.73
2	0.8	3.26	3.31	3.35	3.68
Mean		3.38 ± 0.05	3.40 ± 0.07	3.49 ± 0.06	3.78 ± 0.06

which is also visible in all curves at high temperatures and beyond a shrinkage of 20%.

3.3. Sintering experiments

The sintering experiments in a chamber furnace revealed more realistic and more reliable shrinkage and density data. The sintering curves of series 1 (Fig. 5a) show a rather systematic change with increasing sintering temperature and increasing nominal Zr deficiency.

In the case of $Na_{3.4}Zr_2Si_{2.4}P_{0.6}O_{12}$, the shrinkage curve in Fig. 4 and the densification curve in Fig. 5 correspond to each other, which is characteristic for a polycrystalline material. In all other cases, the stepwise shrinkage is not reflected in Fig. 5 as there is no external pressure [18]. Therefore, in Fig. 5a, the densification curves first show a usual increase with temperature, but continuously shift toward low temperature, and then show a nearly constant high density. Taking the 97% density level as a reference, the samples reach this value at 1245 °C, 1185 °C, 1140 °C, 1105 °C, and 1080 °C from $x = 0$ to $x = 0.8$, respectively. For series 2 (Fig. 5b), the corresponding decrease in sintering temperatures results in 97% density levels at 1245 °C, 1160 °C, 1100 °C, 1030 °C and 1020 °C. A similar systematic change in the density with initially nearly linear increase and then constant high density is observed only for samples with $0 < x < 0.4$. The 2 samples with the expected highest glass content already show a high density at 1000 °C. At higher temperatures, the density gradually decreases again, because the evaporation of Na_2O leads to an increasing fraction of porosity in the samples. This is also the reason why the data show a more pronounced scatter than those of the other samples.

The sintering experiments in the furnace revealed a systematic decrease in the sintering temperature with increasing Zr deficiency in both series. The reason behind this trend is the increasing formation of a glass phase, which acts as a sintering aid [21,25]. Very similar decreases in the sintering temperatures were obtained during the comparison of the sintering properties of materials along the "Hong series" ($Na_{1+z}Zr_2Si_zP_{3-z}O_{12}$) and the "von Alpen series" ($Na_{1+w}Zr_{2-w/3}Si_wP_{3-w}O_{12-2w/3}$) [23]. At this point, it is worth noting that sodium silicate glasses were recently used as sintering aids to densify NaSICON ceramics [46–48].

From a practical point of view, component manufacturing of Zr-deficient NaSICONs can be realized at temperatures that are 100–200 °C lower than for conventional NaSICON materials. However, as already pointed out by Engell et al. [21], the fabrication of dense ceramics with 97% theoretical density is possible at temperatures below 1000 °C, but the crystallinity of such materials is poor. Therefore, to obtain high Na-ion conductivity, a sintering temperature of 1200 °C is usually necessary. In view of these early experiences, the following investigations on the 2 series were performed with samples sintered constantly at 1250 °C, which is also the temperature employed for the material with z = 3.4 [7].

3.4. X-ray diffraction

The XRD patterns of the samples after sintering at 1250 °C were analyzed with the Rietveld refinement technique. The predominant phase is the monoclinic modification (Table 2). The monoclinic lattice parameters do not show a systematic trend in dependence on the stoichiometric variation. In addition, they do not vary strongly indicating a rather narrow homogeneity range of the crystalline phase. Phase analyses of all XRD patterns in the series revealed very weak additional peaks of a minority phase, which could be identified as $Na_3Si_2PO_8$ except for 2 samples. In the case of $Na_{3.4}Zr_2Si_{2.4}P_{0.6}O_{12}$ and $Na_{3.4}Zr_{1.85}Si_{2.35}P_{0.675}O_{11.99}$ small amounts of ZrO_2 were observed as secondary phase. The Rietveld refinements were carried out only for the main phases and the le Bail technique was used to fit secondary phases. This technique is not suitable for quantifying exact phase fractions due to missing essential information on the atomic information of the structure. To obtain the best fit, different volume fractions (in steps of 1 vol%) were applied for the second phase. The results are given in Table 2.

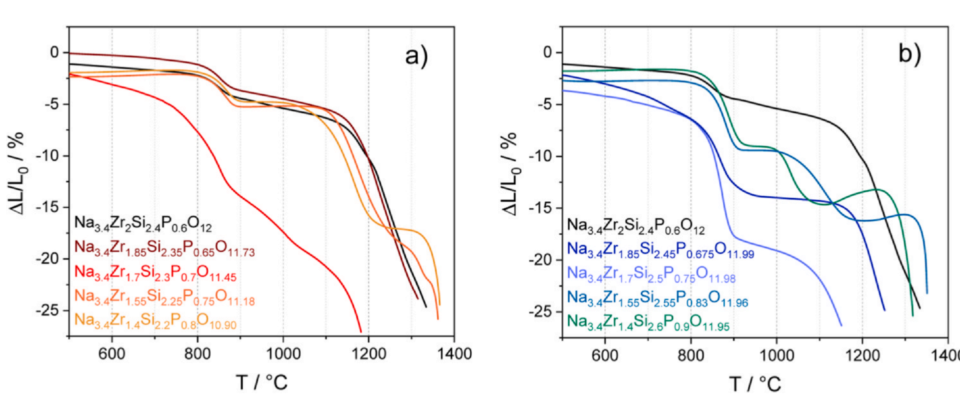

Fig. 4. Dilatometric sintering curves of samples of (a) series 1 and (b) series 2 with a constant heating rate up to 1400 °C.

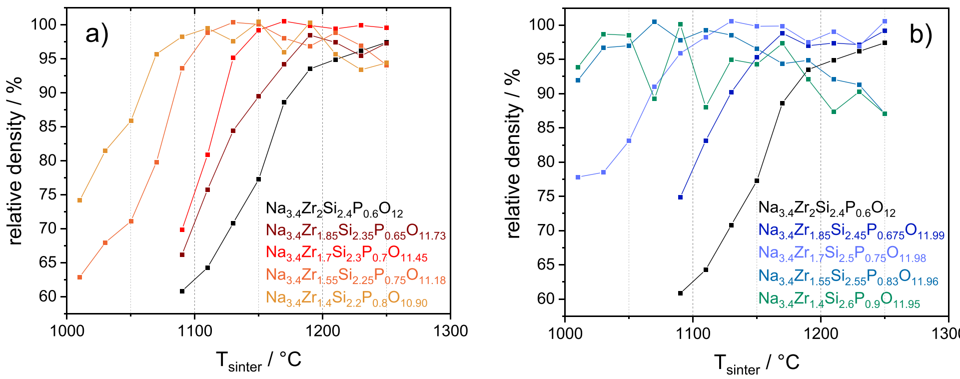

Fig. 5. Relative density of samples of (a) series 1 and (b) series 2 after sintering at various temperatures with a dwell time of 4 h.

To determine the compositional variation of the NaSICON phase, the rhombohedral a_{rh} and monoclinic b_{mon} lattice parameters along the solid solution $Na_{1+z}Zr_2Si_zP_{3-z}O_{12}$ can be used as a calibration curve [21]. Fig. 6 shows the dependence of a_{rh} and b_{mon} on z. The marked range of b_{mon} in light red shows the scatter of the data (Table 2) and the corresponding z values, i.e. the sodium content assuming that the formed crystalline phases belong to the solid solution $Na_{1+z}Zr_2Si_zP_{3-z}O_{12}$. The specific sodium contents are listed in Table 1. All oxygen and Si/P sites were constrained to full occupancy to determine the occupations of Na atoms. Since occupancy for Na1 and Na2 positions tend to be higher than 1, they were also fixed. Only Na3 was freely refined and the results of Na content are given in Table 1. The atomic ratio of Si/P was fixed to agree with the Na content since it is not possible to distinguish the 2 elements here.

3.5. Neutron diffraction

Due to the experimental limitations of XRD, that is, low atomic scattering factors of Na and O and very similar scattering factors of Si and P, neutron diffraction experiments were carried out [51]. They allow the accurate localization and determination of light atoms as well as the determination of the ratio of the randomly distributed Si and P atoms in the polycrystalline phase. The neutron scattering lengths of Na, O, P, Si, and Zr atoms are 3.63 fm, 5.803 fm, 5.13 fm, 4.149 fm, and 7.16 fm, respectively, Furthermore, compared to X-rays, which have a lower penetration power through the material, neutrons are weakly absorbed in matter, penetrating up to several mm into samples to deliver better quantitative information on the main and secondary phase fractions.

As a starting model for Rietveld refinement the crystal structures of both known phases of NaSICON-type materials were used, the monoclinic ($C2/c$) and rhombohedral ($R\bar{3}c$) polymorphs. In preliminary runs, a check was performed to ascertain whether the main diffraction peaks belonged to a single phase of either of these polymorphs or to their mixture. In this first step, zero shift, profile parameters including asymmetry, lattice parameters, and preferential orientations were

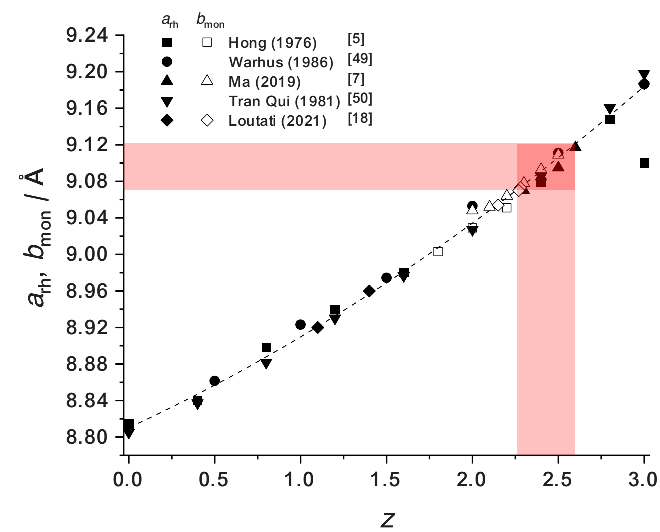

Fig. 6. Dependence of the lattice parameters a_{rh} and b_{mon} on z for the solid solution $Na_{1+z}Zr_2Si_zP_{3-z}O_{12}$. The marked range of b_{mon} in light red shows the scatter of the obtained data (Table 2) and the corresponding z values. The symbols refer to different data sources [5,7,18,49,50] and the dashed line is a polynomial fit of the data.

considered. In the case of the single rhombohedral phase, the wR_p values varied between 4.5% and 7.1%. In the single monoclinic phase and the 2-phase mixture, values were in range of 2.1–3.1% and 2.3–6.94%, respectively. Based on these wR_p values and the previous XRD results, the main phase in all samples was refined as a monoclinic NaSICON phase. In addition, the diffractograms contain few weak reflections of minority phases. Further analyses of these weak additional reflections showed that the minority phase can be identified as $Na_3Si_2PO_8$ (ISCD 161804) as a crystallization product of the glassy phase. One sample (with x = 0) revealed peaks of ZrO_2 as a secondary phase (Table 3).

Table 2
Monoclinic lattice parameters and phase fractions (in the sequence NaSICON/$Na_3Si_2PO_8$/ZrO_2) determined by XRD.

Series	x	a / Å	b / Å	c / Å	β / °	V / Å³	Phase fraction / %
1 + 2	0	15.7697 (11)	9.1198 (6)	9.2347 (6)	124.3 (1)	1097.0 (1)	99 / – / 1
1	0.2	15.7065 (8)	9.0867 (5)	9.2305 (5)	124.0 (1)	1092.3 (1)	99 / 1 / –
1	0.4	15.7346 (12)	9.0942 (7)	9.2241 (6)	124.2 (1)	1091.9 (2)	99 / 1 / –
1	0.6	15.9307 (30)	9.0709 (10)	9.1929 (19)	124.4 (1)	1096.4 (5)	80(5) / 20 / –
1	0.8	15.7109 (10)	9.0893 (5)	9.212 (5)	124.2 (1)	1088.5 (1)	99 / 1 /–
2	0.2	15.6921 (11)	9.0859 (7)	9.222 (6)	124.0 (1)	1088.4 (1)	90(5) / – / 10
2	0.4	15.7182 (11)	9.0938 (6)	9.2294 (6)	124.0 (1)	1093.0 (1)	99 / 1 / –
2	0.6	15.735 (20)	9.1062 (13)	9.2263 (14)	124.2 (1)	1093.7 (3)	99 / 1 / –
2	0.8	15.6917 (30)	9.0783 (18)	9.2315 (18)	123.9 (1)	1091.4 (4)	95(5) / 5 / –

Table 3
Lattice parameters, phase fractions, and residual values of refinements for the NaSICON samples determined by ND.

Series	x	Refined composition	a / Å	b / Å	c / Å	β / °	V / Å^3	NaSICON fraction / %	Impurity	wR_2, wR_p
1 + 2	0	$Na_{3.62}Zr_{1.95}Si_{2.4}P_{0.6}O_{12}$	15.7859 (4)	9.1241 (2)	9.2126 (2)	124.4 (1)	1095.14 (5)	98 (1)	ZrO_2	2.95, 3.75
1	0.2	$Na_{3.56}Zr_{1.95}Si_{2.35}P_{0.65}O_{12}$	15.7655 (5)	9.1142 (3)	9.2282 (3)	124.2 (1)	1096.35 (6)	100 (1)	-	2.96, 3.84
1	0.4	$Na_{3.58}Zr_{1.93}Si_{2.3}P_{0.7}O_{12}$	15.7741 (4)	9.1172 (2)	9.2274 (2)	124.3 (1)	1096.53 (5)	83 (1)	$Na_3Si_2PO_8$	2.31, 2.98
1	0.6	$Na_{3.47}Zr_{1.95}Si_{2.25}P_{0.75}O_{12}$	15.7499 (5)	9.1076 (3)	9.2314 (3)	124.1 (1)	1096.10 (6)	90 (1)	$Na_3Si_2PO_8$	2.53, 3.28
1	0.8	$Na_{3.47}Zr_{1.93}Si_{2.2}P_{0.8}O_{12}$	15.7505 (5)	9.1081 (3)	9.2332 (3)	124.1 (1)	1096.40 (6)	93 (1)	$Na_3Si_2PO_8$	2.59, 3.38
2	0.2	$Na_{3.47}Zr_{1.96}Si_{2.32}P_{0.68}O_{12}$	15.7362 (3)	9.1008 (2)	9.2416 (2)	124.0 (1)	1097.04 (4)	86 (4)	$Na_3Si_2PO_8$	2.62, 3.40
2	0.4	$Na_{3.44}Zr_{1.95}Si_{2.25}P_{0.75}O_{12}$	15.7292 (4)	9.0976 (2)	9.2395 (2)	124.0 (1)	1096.45 (5)	90 (1)	$Na_3Si_2PO_8$	2.38, 3.04
2	0.6	n. a.	–	–	–	–	–	–	–	–
2	0.8	$Na_{3.35}Zr_{1.94}Si_{2.1}P_{0.9}O_{12}$	15.7048 (5)	9.0845 (3)	9.2388 (3)	123.9 (1)	1094.68 (6)	69 (2)	$Na_3Si_2PO_8$	2.30, 3.01

In the second step of the refinements, all atomic positions for the main and minority phases were refined. In addition, the SOF and thermal displacement parameters (TDP) of oxygen atoms were checked carefully for the main phase. All oxygen atoms showed full occupation with reasonable TDP parameters. Therefore, SOF for oxygen atoms was fixed to be 1.

In the next step, the TDP for statistically distributed Si and P atoms were considered for 2 fully occupied atomic sites at *4e* and *8f*. When the TDP for Si/P atoms was constrained to be equal, the refinement of SOF resulted in reasonable values close to those expected from the nominal composition. In further cycles of the refinement, the SOF of Si/P sites were therefore fixed to stoichiometries with full occupation. The observed and calculated ND patterns after final refinement are shown in the Supplementary information (Fig. S1).

Several structure models for the monoclinic NaSICON phase (*C*2/*c*, SG. 15) are described in the literature with different numbers of Na atoms as shown in Table 4. Na atoms are located at 3 different Wyckoff sites, *4d* (1/4,1/4,1/2) (Na1), *4e* (1/2,y,1/4) (Na2), and *8f* (x,y,z) (Na3). The *4e* site is mostly fully occupied whereas *4d* and *8f* sites tend to be partly filled. In addition, there are structural models with 1 (Na4) [52] or 2 (Na4, Na5) [53] additional Na positions on *8f* sites. In our refinements, the sites *4e* and *8f* tended to full occupation similar to reported Zr-deficient NaSICONs [54–56]. In this work, the occupancies of Zr sites were refined without constraints and always resulted in values less than unity between 0.93 and 0.98 according to the compositions given in Table 3. A mixed Zr/Na occupancy of the Zr site as described earlier [54] did not significantly change TDP and resulted in slightly increased wR_p values of up to 4.5%.

Likewise, refining a Zr/Si mixed occupancy also yielded wR_p values of up to 5%. From the chemical point of view, the occupation of this site with Si is unlikely, because sixfold-coordinated Si^{4+} ions are very rare. Therefore, this structure model was discarded. Instead, the presence of Na^+ on Zr sites is very likely, because the additional Na^+ ions stabilize the structure in comparison to vacancies. For further discussion, however, the structure model with the lowest wR_p values is used.

In the refinements, the Fourier difference maps showed no residual scattering density that could be assigned to Na4 and Na5sites, thus only the occupancies at 3 Na atomic positions were refined. Both Na2 and Na3 occupancies were refined to values slightly above 1, therefore they were fixed to be fully occupied. The SOF of Na1 was found to be less than 1 for all refined compositions, with values close to the corresponding charge-balanced formula. Therefore, the SOF of Na1 was fixed to match this stoichiometry in the final cycles of refinement.

The crystal structure of NaSICON materials consists of the polyanionic framework of (Si,P)O_4 tetrahedra corner-shared with ZrO_6 octahedra and Na cations sitting in the cavities. Since the ionic radius of Si in tetrahedral coordination (0.26 Å) is slightly larger than that of P (0.17 Å) [61], the size of the cavities widens with increasing Si content, and therefore the maximum amount of Na cations is expected in the Si-rich compositions in the series investigated here.

Anisotropic thermal parameters for Zr atoms and Na atoms gave negative values, thus they were refined isotropically. Introducing anisotropy of O atoms did not significantly improve the R-values. The isotropic thermal displacements for Na3 atoms were large, almost one order of magnitude higher than Na1 and Na2, indicating their high mobility.

No significant variation was obtained for the averaged bond lengths (Table 5). A detailed table of refined atomic positions, isotropic displacement parameters, and site occupancy factors are listed in Table S2. The bond lengths for the individual samples are shown in Table S3. The bond lengths do not show a significant tendency related to the variation of the elements. Therefore, the crystal structure and also the composition of the crystalline phase do not vary much, indicating a stable 2-phase region in the investigated area of the phase diagram. The interionic distances also agree very well with those determined from previous structure refinements with similar compositions, either with or without Zr deficiency [5,52,55,56,59].

Table 4
Occupancies of Na and Zr sites in different monoclinic NaSICON compounds. Values in italics indicate the refinement of the same dataset using different structure models[a,b,c,d].

Composition	T / K	Na1 (4d)	Na2 (4e)	Na3 (8 f)	Na4(8 f)	Na5(8 f)	Zr1 (8 f)	Ref.
$Na_3Zr_2Si_2PO_{12}$	293	1	1	0.50			1	[5]
		0.60	1	0.69			1	[53]
		0.58	1	0.83			1	[57]
$Na_{3.12}Zr_2Si_{2.12}P_{.88}O_{12}$	293	0.22	1	0.56	0.39		1	[52]
$Na_3Zr_2Si_2PO_{12}$:	3	*0.98*	*0.89*	*0.54*	*0.44*	*0.10*	*1*	[57]
$Na_{2.95}Zr_2Si_2PO_{12}$[a]		*0.47*	*0.76*	*0.59*	*0.46*		*1*	
$Na_{2.41}Zr_2Si_2PO_{12}$[b]		*0.38*	*1*	*0.14*			*1*	
$Na_{2.54}Zr_2Si_2PO_{12}$[c]		*0.22*	*0.86*	*0.38*			*1*	
$Na_{2.96}Zr_2Si_2PO_{12}$[d]								
$Na_{2.88}(Na_{.32}Zr_{1.68})Si_{1.84}P_{1.16}O_{11.54}$	293	0.27	1	0.80			0.84 (+0.16 Na)	[54]
$Na_{3.24}Zr_{1.956}Si_2PO_{12}$	293	0.58	1	0.83			0.98	[55]
$Na_{3.29}Zr_{1.936}Si_2PO_{12}$	293	0.48	1	0.91			0.97	[55]
$Na_{2.41}Zr_2Si_{1.88}P_{1.14}O_{12}$	293	0.22	0.94	0.62			1	[58]
$Na_3Zr_{1.93}Si_2PO_{12}$	293	0.22	1	0.89			0.97	[56]
$Na_{3.17}Zr_{1.93}Si_{1.91}P_{1.09}O_{12}$	293	0.27	1	0.95			0.97	[56]
$Na_{3.31}Zr_{1.67}Si_{1.84}P_{1.16}O_{12}$	293	0.83	0.98	0.75			0.84	[56]
$Na_3Zr_2Si_2PO_{12}$	293	0.81	1	0.60			1	[59]
$Na_3Zr_2Si_2PO_{12}$	300	0.24	0.88	0.38	0.44	0.12	1	[53]
$Na_3Zr_2Si_2PO_{12}$	3	0.07	1	0.24	0.58	0.16	1	[53]
$Na_3Zr_2Si_2PO_{12}$	293	0.22	1	0.50	0.39		1	[60]

[a] Starting model from [59], only Na site occupancies refined.
[b] Starting model from [59], Na site occupancies, all atom positions, and TDP refined.
[c] Starting model from [52], only Na site occupancies refined.
[d] Starting model from [53] (300 K data), only Na site occupancies refined. This model is considered to be most suitable by the authors [57] because other models result in unstable refinement or significant differences between refined and nominal composition.

Table 5
Selected averaged distances (in Å) in NaSICON structure of the investigated compositions.

		Series 1				Series 2		
	x = 0	x = 0.2	x = 0.4	x = 0.6	x = 0.8	x = 0.2	x = 0.4	x = 0.8
Zr – O	2.082	2.088	2.086	2.088	2.086	2.081	2.081	2.087
Si1|P1 – O	1.6098	1.6033	1.6061	1.5997	1.6049	1.6002	1.6017	1.5987
Si2|P2 – O	1.6030	1.5933	1.5894	1.5964	1.5928	1.6053	1.6043	1.5795
Na1 – O	2.637	2.635	2.652	2.668	2.664	2.678	2.682	2.701
Na2 – O	2.613	2.618	2.619	2.606	2.607	2.603	2.601	2.585
Na3 – O	2.616	2.555	2.565	2.575	2.573	2.569	2.568	2.577
Na1 – Na3	2.9623	2.7655	2.7499	2.6941	2.7000	2.6513	2.5543	2.6778
Na1 – Na2	3.5012	3.5267	3.5100	3.5266	3.5267	3.4944	3.5141	3.5261

After proclamation of the solid solution $Na_{1+w}Zr_{2-w/3}Si_wP_{3-w}O_{12-2w/3}$ [20,62], few groups dedicated work on these Zr-deficient NaSICON materials. Engell et al. [21] carefully investigated 11 compositions — 4 of them with Zr deficiency — synthesized by the sol-gel method. One of the compositions (NZPS-82-1BC; $Na_{2.94}Zr_{1.49}Si_{2.2}P_{0.8}O_{10.85}$) was obtained with 97% theoretical density at temperatures below 1000 °C but with poor crystallinity. To achieve high ionic conductivity, the material had to be sintered at 1200 °C. Another compound (NZS-80-2; $Na_{4.06}Zr_{1.06}Si_3O_{10.14}$), comparable with the end member of the above solid solution (w = 3), was clearly identified as rhombohedral NaSICON ($Na_4Zr_2Si_3O_{12}$) with only minor Zr deficiency and a glass phase. In a subsequent paper [22], the authors again investigated the batch NZPS-82-1BC and determined the crystalline phase as $Na_{3.18}Zr_2Si_{2.18}P_{0.82}O_{12}$ after sintering at 1250 °C and another Zr-deficient material (NZPS-79-6.4,2.1; $Na_{2.85}Zr_{1.7}Si_2PO_{11.32}$) which gave a crystalline NaSICON phase ($Na_{2.89}Zr_2Si_{1.89}P_{1.11}O_{12}$) and an interstitial glass with about 15 vol%. In comparison to Table 3, the slightly smaller lattice parameters of both compounds reflect the lower sodium content.

Perthuis and Colomban [24,63] also investigated the material with the composition $Na_{3.1}Zr_{1.55}Si_{2.3}P_{0.7}O_{11}$ and concluded that the expected and observed stoichiometry showed a large discrepancy and that the nominal formula is incorrect if the samples are monophasic. Applying thermal treatments above 1100 °C led to decreasing intensity of NaSICON reflections and the formation of additional phases, in particular a vitreous phase.

Since the Zr-deficient NaSICON materials obviously always contain a substantial amount of glass, similar compositions were prepared as vitreous solid electrolytes by purpose. As an example, a glass with the composition $Na_4ZrSi_3O_{10}$ had a similar ionic conductivity at 300 °C to the crystalline material [64], whereas the conductivity in [65] is about one order of magnitude lower.

Parallel to the work on ceramics just mentioned, there was intense crystallographic research on single crystals as well on polycrystalline materials. Kohler et al. [66,67] refined XRD data to determine the crystal structure of a NaSICON crystals resulting in the composition $Na_{3.1}Zr_{1.78}Si_{1.24}P_{1.76}O_{12}$. They suggested a new composition plane allowing Zr deficiency for the NaSICON compounds and corresponding to the rear blue triangle in Fig. 1a. They assumed that the Zr site cannot be occupied by Na. They observed different lattice parameters (a ≈ 9.05 Å, c ≈ 23 Å at 150–220 °C) than those of $Na_3Zr_2Si_2PO_{12}$ (e.g., [5]). In [68], Kohler and Schulz described a Zr-deficient $Na_4Zr_{2-x}Si_3O_{12}$ crystal assuming that the missing charges are compensated by OH^- groups.

Rudolf et al. [54] hydrothermally synthesized a powder with composition $Na_{2.88}(Na_{0.32}Zr_{1.68})Si_{1.84}P_{1.16}O_{11.54}$ after structural refinement with explicit replacement of Zr^{4+} by Na^+ ions and shared site occupancy of the Zr site. The application of XRD and ND allowed the refinement of the Si/P ratio. Lattice parameters were a = 15.6209(8), b = 9.0326(5), c = 9.2172(5) Å, β = 123.67(1) °, V = 1082.5 Å^3. The occupancy factors of oxygen did not indicate any tendency toward vacancy formation.

In [56], Rudolf et al. investigated 3 materials by ND: a sol-gel prepared NaSICON with formula $Na_3Zr_{1.93}Si_2PO_{11.86}$, a commercial and reheated sample with composition $Na_{3.17}Zr_{1.93}Si_{1.9}P_{1.1}O_{12}$, and a sample with similar stoichiometry as reported before [54] ($Na_{3.31}Zr_{1.67}Si_{1.85}P_{1.15}O_{11.57}$) but prepared by the sol-gel method (a = 15.6736(2), b = 9.0669(1) c = 9.2207(1) Å, β = 123. 843(4) °, V = 1088.34(2) Å^3). In the latter case, there was no evidence for the presence of Na^+ on the Zr site and strong separation of Si and P among the polyanionic sites. Rudolf et al. suggested the general formula $Na_{1+4a+z}Zr_{2-a-f}Si_zP_{3-z}O_{12-2f}$, where "f" represents the ZrO_2 molar deficiency and "a" the amount of Zr^{4+} vacancies compensated by 4 Na^+ ions. They also proposed that the synthesis method and thermal history is largely responsible for the observed crystallographic differences.

Lucco-Borlera et al. [27] synthesized samples of $Na_3Zr_{2-e/4}Si_{2-e}P_{1+e}O_{12}$ with 0.333 < e < 1.667 and determined the lattice parameters from XRD powder patterns, but did not analyze other crystallographic information like site occupancies. They also did not comment on the formation of glass phases. Since no further structural or microstructural details are given, their lattice parameters can also be interpreted with Fig. 6, and the resulting compositions in the series $Na_{1+z}Zr_2Si_zP_{3-z}O_{12}$ correlate linearly according to z = (2.32 ± 0.12)–(0.97 ± 0.11) × e with R^2 = 96.5%. It is important to note that the investigated series is orthogonal to the 2 series investigated here (see Fig. 1b).

Traversa et al. [69] also reported the properties of $Na_3Zr_{2-e/4}Si_{2-e}P_{1+e}O_{12}$ with e = 0, 0.667, and 1.333. The crystallographic investigation was restricted to the determination of the lattice parameters. However, they also reported the formation of a glass phase for compositions with $e > 0$ as well as an accelerated densification at a low sintering temperature of 1100 °C. When applying the calibration curve in Fig. 6 here, the alternative compositions in the series $Na_{1+z}Zr_2Si_zP_{3-z}O_{12}$ can be calculated with z = (1.95 ± 0.04)–(1.66 ± 0.10) × e with R^2 = 99.6%.

The material with the highest Zr deficiency is $Na_5ZrP_3O_{12}$, whereas $Na_4ZrSi_3O_{10}$ does not seem to exist. The structure determination of $Na_5ZrP_3O_{12}$ was carried out on single crystals [70] and clearly demonstrated the substitution mechanism of 4 Na^+ ions for one Zr^{4+} ion, in which one-fourth of the Na^+ ions occupy Zr sites. An additional small substitution of P with Si was also reported ($Na_{5.3}ZrSi_{0.3}P_{2.7}O_{12}$) requiring an additional interstitial site for the Na^+ ions [71].

The previous results described above do not give a clear view of the site occupancy of the Zr position. An occupancy with additional Na^+ ions was only observed for hydrothermally synthesized powder [54] and for compositions with very high Zr deficiency [70,71] to stabilize the NaSICON structure. When only a small number of Zr vacancies (up to 10–15%) are present, the diffraction results and the refined structure models did not give a clear indication of Na^+ ions on the Zr position.

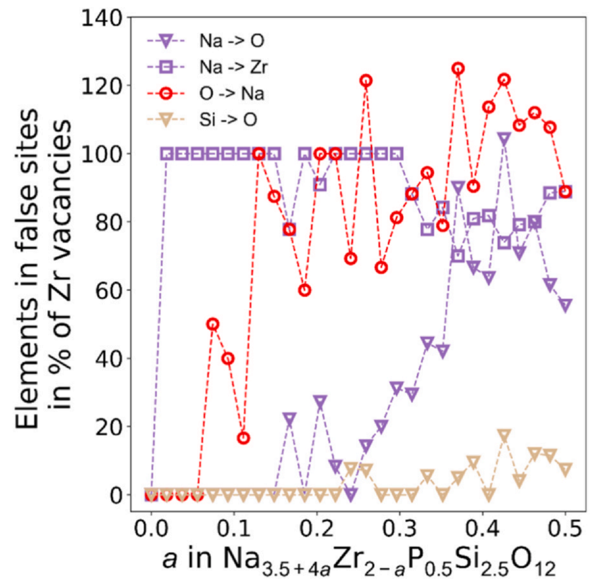

Fig. 8. Fraction of ions occupying false sites (relative to the number of available Zr vacancy sites). At low vacancy concentrations, only Na occupies false sites, namely the vacant sites of Zr. With increasing vacancy concentration, other elements also start occupying false sites eventually leading to a collapse of the NaSICON structure. The occurrence of O on Na sites at around a = 0.2 may explain the kink in the mixing energy in Fig. 7.

The R-values with and without Zr/Na-site occupation do not differ very much, probably due to the large TDPs of the Na^+ ions. From the energetic point of view, a stabilization of the structure with Na^+ on Zr sites can be expected for any level of Zr deficiency.

3.6. Atomistic modeling

For a better understanding of the thermodynamic stability of Zr vacancies, their compensation, and their influence on local atomic structure, atomistic simulations were performed (for details see Experimental Section) based on configurations of $Na_{1+z}Zr_2Si_zP_{3-z}O_{12}$ with (and without) Zr vacancies and constructed from the reference structure of Boilot et al. [72] with z = 2.5. Although this does not fully match the experimental composition, atomistic models can be represented in any repeat unit of the conventional unit cell; for z = 2.4, a repeat unit (supercell) of 5 × 5 × 2 with respect to the unit cell would be required (for roughly equal lengths of the supercell vectors, ensuring isotropy). Here, for z = 2.5, a smaller repeat unit of 3 × 3 × 1 unit cells was chosen having also equal lengths of the supercell vectors. For the

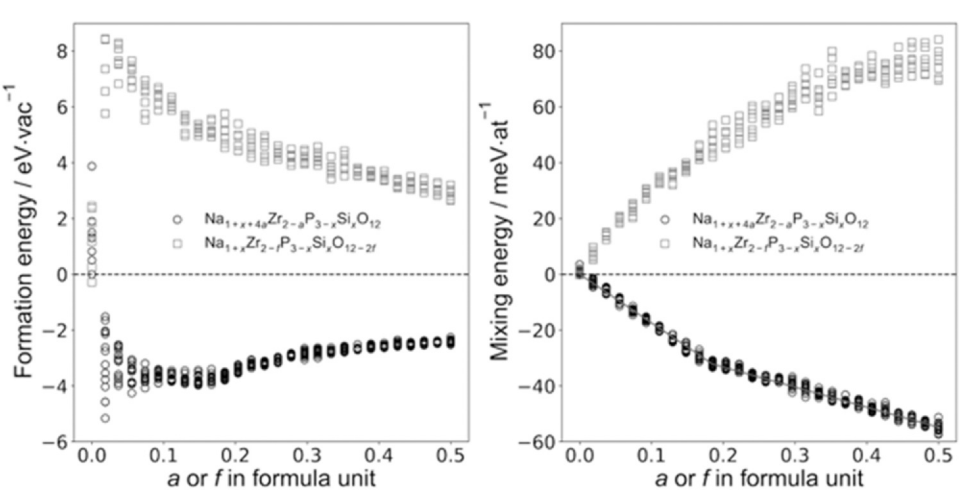

Fig. 7. Zr^{4+} vacancy formation energies for $Na_{1+z+4a}Zr_{2-a}P_{3-z}Si_zO_{12}$ (compensation via 4 Na^+) and $Na_{1+z}Zr_{2-f}P_{3-z}Si_zO_{12-2f}$ (compensation via 2 V_O^{2+}) as a function of the vacancy concentration a or f. Zr^{4+} vacancies compensated via excess Na^+ are found to be energetically favorable (negative formation energy); compensation via additional O^{2-} vacancies is not favorable.

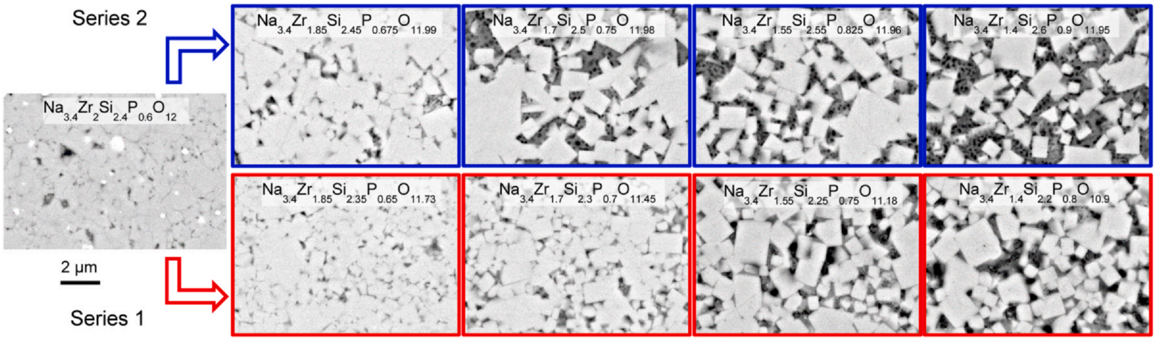

Fig. 9. SEM micrographs in back-scattering mode of the investigated NaSICON materials. The crystalline and glassy phase fractions appear as light and dark gray areas, respectively. The black dots inside the gray areas are pores created by the evaporation of Na_2O during sintering.

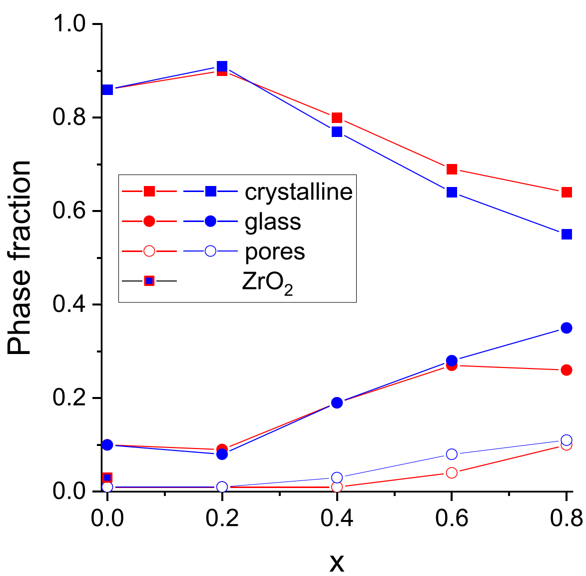

Fig. 10. Phase fractions determined by image analysis of the SEM micrographs of the investigated NaSICON materials. The red and blue symbols correspond to series 1 and series 2, respectively.

pristine case (no vacancies), 14 replicas with random distributions of Si, P, and Na were prepared using the atomic simulation environment [73]. For systems with Zr vacancies (V_{Zr}^{4-}), 2 compensation mechanisms were considered: (i) compensation of one V_{Zr}^{4-} by 4 additional Na^+ ions ($Na_{1+z+4a}Zr_{2-a}P_{3-z}Si_zO_{12}$) and (ii) compensation of one V_{Zr}^{4-} by 2 oxygen vacancies V_O^{2+} ($Na_{1+z}Zr_{2-f}P_{3-z}Si_zO_{12-2f}$). In case one, for each value of a, we either distribute all Na ions on Na sites or one Na out of 4 on the V_{Zr}^{4-} sites and the 3 remaining ones on Na sites. For the 3 scenarios, 7 replicas were prepared for every value of a. All systems were then equilibrated in isobaric-isothermal (constant particle number, constant pressure, constant temperature, *NpT*) simulations ($p = 0$) where the temperature was ramped from 300 K to 700 K within 8 ps, kept constant for 50 ps, cooled down to 100 K within 12 ps and finally optimized at zero K. Then the thermodynamic stability was analyzed by means of defect formation energies and structural investigations. The defect formation energies were calculated as (compensation via Na^+ ions)

$$E_f = [E(Na_{1+z+4a}Zr_{2-a}P_{3-z}Si_zO_{12}) + a\,E(ZrO_2) - E(Na_{1+z}Zr_2P_{3-z}Si_zO_{12}) - 2\,a\,E(Na_2O)]\;/\;a \quad (1)$$

or (compensation via V_O^{2+})

$$E_f = [E(Na_{1+z}Zr_{2-f}P_{3-z}Si_zO_{12-2f}) + f\,E(ZrO_2) - E(Na_{1+z}Zr_2P_{3-z}Si_zO_{12})]\;/\;f \quad (2)$$

Here, E(system) is the total energy of the system given in parenthesis and a or f is the number of Zr vacancies. For the energy of pristine NaSICON ($Na_{1+z}Zr_2P_{3-z}Si_zO_{12}$), the average energy over all 14 replicas was used.

Fig. 7 shows the calculated defect formation energies. Obviously, the data show a relatively large scatter, in particular at low Zr deficiencies. This is due to the random character of themodels as well as their size (~1000 atoms per cell). An energy difference of only 1 meV/atom between 2 models amplifies to 1 eV per cell. In fact, the standard deviation among all pristine NaSICON models is 1.2 eV/per cell. With increasing vacancy concentration, the scatter is reduced due to the normalization with respect to the number of vacancies in the system. The simulations clearly show that the compensation of a Zr vacancy by additional Na is preferred rather than the compensation by additional oxygen vacancies (given that Na_2O is available). The formation of a ZrO_2 vacancy complex is accompanied by an energy barrier of 6–4 eV/formal unit so that its occurrence can be practically neglected. Instead, compensation of the Zr vacancy via Na excess results in negative formation energy. The Na ions always automatically relaxed onto free Zr vacancies independent of the starting configuration. As such, $Na_{1+z+4a}Zr_{2-a}P_{3-z}Si_zO_{12}$ is not a NaSICON with vacancies, but the thermodynamically favored phase, if Na is available during synthesis. Therefore, the mixing energy is also plotted in Fig. 7. The mixing energy is obtained from Eqs. (1) or (2) by normalization with the total number of atoms in the cell instead of the number of vacancies. The red line is an attempt to draw the convex hull. Apparently, regarding the accuracy and scatter of the data, all compositions lie on the convex hull up to the maximum value of $a = 0.5$ considered here and must be regarded as stable against pristine NaSICON, ZrO_2 and Na_2O. However, at about $a = 0.2$, there is a kink in the convex hull, which requires a more in-depth structural analysis.

Changes in the site occupancies were investigated by comparing the optimized low-energy $Na_{1+z+4a}Zr_{2-a}P_{3-z}Si_zO_{12}$ structures with the reference crystal structure [72]. This is achieved by rescaling the latter to the lattice parameters of the former, overlaying the structures and identifying the atom of chemical species Y of the prototype structure that is closest to every atom of species X in the $Na_{1+z+4a}Zr_{2-a}P_{3-z}Si_zO_{12}$ structure. If Y is not identical to X, then X occupies a Y site. Fig. 8 shows the fraction of various species in $Na_{1+z+4a}Zr_{2-a}P_{3-z}Si_zO_{12}$ that occupy false sites (a Y site instead of an X site). For low concentrations of Zr vacancies, only Na occupies false sites, namely the site of the vacancy.

With increasing vacancy concentration, the first oxygen atoms start occupying Na sites, then Na occupies oxygen sites, and finally Si also occupies oxygen sites. At around $a = 0.2$ sodium ions start to populate oxygen sites (purple triangles) and simultaneously there is a drastic change in the number of oxygen ions occupying sodium sites (red circles). This indicates the collapse of the structure and explains the kink in the mixing energy.

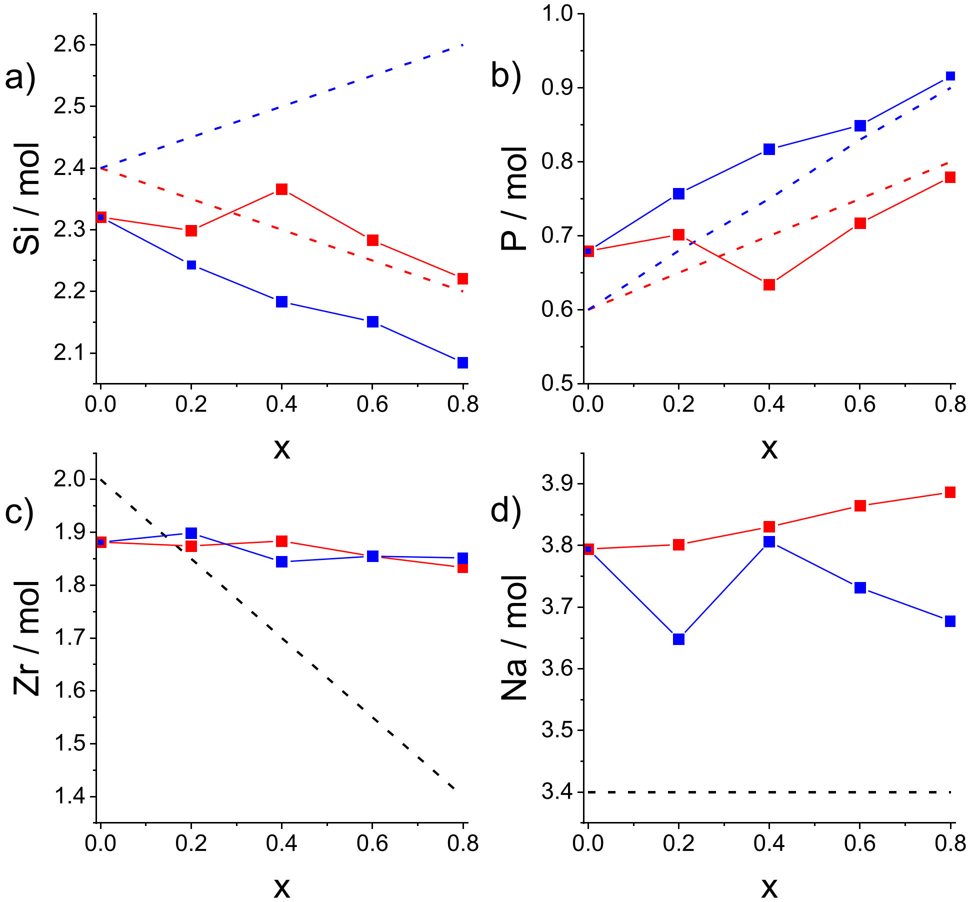

Fig. 11. (a-c) Analytical composition (mol per formula unit) of the elements Si, P, and Zr determined by EDX (red symbols for series 1 and blue symbols for series 2). (d) The Na contents were calculated on the basis of the 3 elements normalized to full occupancy of the polyanionic content ($n_{Si} + n_P = 3$). The dashed lines represent the nominal trend of the elements according to series 1 (red) and series 2 (blue) and to both series (black).

3.7. Microstructural investigations

The microstructure of the 9 NaSICON materials was investigated by scanning electron microscopy (SEM) using polished cross sections (Fig. 9). In the case of $Na_{3.4}Zr_2Si_{2.4}P_{0.6}O_{12}$, the crystalline particles have a diameter of about 1–2 µm, and a small amount of ZrO_2 particles can be observed as white circular grains. With increasing x, the NaSICON particles increase in size when they are embedded in the glassy phase (visible as dark gray areas in Fig. 9). The grain growth is the largest for the samples with $x = 0.4$ and 0.6 in series 2. Additionally, the phase fraction of the glassy compounds increases with x. This was confirmed quantitatively by image analysis of the areas with different gray scales (Fig. 10). In this way, the amount of nano-porosity was also detected (black dots in the SEM micrographs, Fig. 9) which explains the decreasing density at high sintering temperatures (Fig. 5). For image analysis, micrographs with a lower magnification than those shown in Fig. 9 were used in order to obtain a wider picture of the microstructure that is as representative as possible. In general, samples from series 1 showed a rather homogeneous microstructure with narrow grain size distribution and glass phase around all grains, while the samples from series 2 had a distinctly heterogeneous structure (broad grain size distribution, irregular distribution of the minor phase). It is interesting to note that the crystalline phase fraction in the samples with $x = 0.2$ is slightly higher than in the sample with $x = 0$. This can be explained, on the one hand, by the disappearance of the ZrO_2 and, on the other hand, by an extended stability region of the NaSICON phase itself. Beyond this Zr deficiency level, the materials have a pronounced 2-phase character and can be regarded as glass-ceramic composites.

The chemical composition of the NaSICON grains was quantitatively analyzed with EDX using $ZrSiO_4$ and $Ca_3(PO_4)_2$ as standard materials for calibration. The sodium content was not analyzed due to the strong interaction of the specimens with the electron beam resulting in an unstable Na signal [74]. Hence, the Na content was calculated on the basis of the contents of Si, P, and Zr, assuming full occupancy of the polyanionic sites ($n_{Si} + n_P = 3$) and no oxygen vacancies. The analytical content of Si decreases with increasing x for both series (Fig. 11a), even though the nominal values increase for series 2. This results in a strong deviation from the nominal composition and to a substantial amount of SiO_2 that is available for glass formation. In the case of phosphorus, the nominal amounts increase for both series and the analytical results follow this trend with initial deviations up to $x = 0.4$ (Fig. 11b). Therefore, the offered P_2O_5 amount is incorporated to a large extent into the crystalline phase. The normalization of the polyanionic occupancy with Si and P leads to stable Zr contents varying between $1.83 < n_{Zr} < 1.90$ ($\bar{n}_{Zr} = 1.864 \pm 0.020$); Fig. 11c) despite the fact that the nominal contents decrease in the same way for both series. As a result, these values explain very clearly 1) the precipitation of ZrO_2 in the starting composition, 2) the very low glass content in Figs. 9 and 10 for the samples with $x = 0.2$, because here the analytical compositions correspond to the nominal content, and 3) the significantly increasing glass content in the samples with $x > 0.2$, because the crystalline phase absorbs much more ZrO_2 than anticipated, leading to a reduced NaSICON fraction. The analytical Zr results suggest very consistent and thermodynamically quasi-equilibrated phase formation, revealing NaSICON compositions with a nearly constant Zr deficiency of 5–8%, which is in good agreement with the ND results. The calculated sodium contents vary between 3.65 and 3.9 mol/formula unit (Table 1, Fig. 11d) and are significantly higher than the values obtained by DSC and XRD (see Table 1), because the calculated amounts contain additional sodium (0.4–0.67 mol/formula unit) due to the charge compensation of the Zr deficiency. Also in the case of the ND refinements, additional charge-compensating sodium amounts (0.15–0.3 mol/formula unit) lead to higher sodium contents than those obtained by DSC and XRD measurements (see Table 1). If these charge-

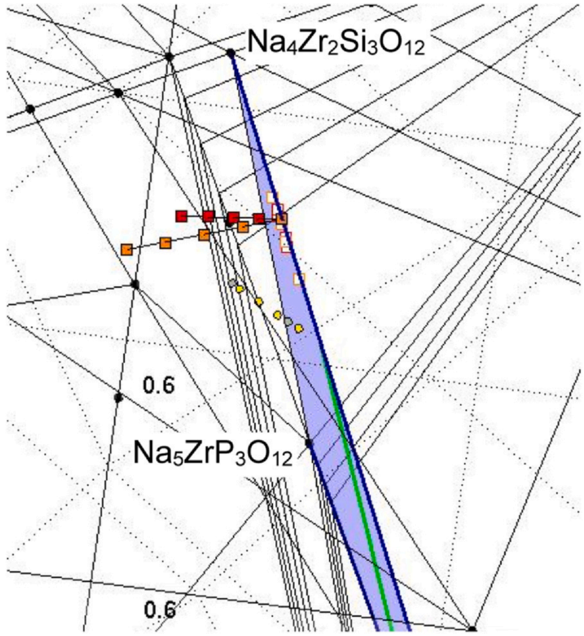

Fig. 12. Quarternary phase diagram showing the nominal starting compositions (series 1 and series 2 as red and orange squares, respectively) and the resulting NaSICON compositions determined by ND (white squares with red and orange edging). The NaSICON region is now restricted to the blue triangle made up of the compositions $NaZr_2P_3O_{12}$-$Na_4Zr_2Si_3O_{12}$-$Na_5ZrP_3O_{12}$ shown here with a small deflection from the in-plane line to visualize the deviation of the other symbols. For comparison, the green line corresponds to the series $Na_3Zr_{2-e/4}Si_{2-e}P_{1+e}O_{12}$ [27,69] and the small yellow and gray circles belong to the nominal compositions using $Na_2Si_2O_5$ and Na_2SiO_3 as a sintering aid for densification of $Na_3Zr_2Si_2PO_{12}$, respectively [46–48].

compensating sodium amounts are subtracted from the experimentally determined values, then the mean Na contents result in 3.38 ± 0.05, 3.40 ± 0.07, 3.24 ± 0.08, and 3.28 ± 0.09 mol per formula unit of $Na_{1+z}Zr_2Si_{2+z}P_{1-z}O_{12}$ for DSC, XRD, ND, and EDX, respectively. This shows that the Na contents are very similar, when Zr vacancies are neglected. Overall, the values in Table 1 show that there is no systematic dependence on x or z. Interestingly, however, is the fact that the experimental results closely meet the nominal Na content of the samples.

Due to the instable Na signal during the EDX measurements, the glass phase could not be analyzed. To provide an impression of the possible phase formation, the phase fractions were calculated on the basis of the neutron diffraction refinements (Table 3), which were subtracted from the nominal compositions. The calculations are outlined in the Supporting information (Table S4). According to the obtained results so far, the Zr content is absorbed in the crystalline phase and the glass is mainly composed of Na, Si, and a smaller amount of P. A first indication of the glass chemistry can be obtained from the Na_2O-SiO_2-P_2O_5 ternary system [75,76]. The observed melting points of the glass phase (1045–1070 °C; Fig. 3) can be found in the ternary system in 2 regions: a) along the tie line Na_2SiO_3–Na_3PO_4 between Na_2SiO_3 (melting point 1088 °C) and the eutectic point (1020 °C) at 81.4 mol% Na_2SiO_3 and 18.6 mol% Na_3PO_4 and b) along the tie line $Na_2Si_2O_5$–Na_3PO_4 between 55 mol% and 65 mol% $Na_2Si_2O_5$ with a maximum melting temperature of 1100 °C for the composition $Na_{18}P_4Si_6O_{31}$ [75]. From the liquidus lines, the relevant compositional regions can be expressed as a) $Na_{2+g}Si_{1-g}P_gO_{3+g}$ with $0.028 < g < 0.078$ and b) $Na_{2+g}Si_{2-2g}P_gO_{5+3g}$ with $0.33 < g < 0.36$ and $0.42 < g < 0.45$, as indicated in Fig. S4.

Since the glass fraction is steadily increasing with the nominal Zr deficiency, this phenomenon offers several advantages for battery development. On the one hand, the amount of glass can be optimized for the sintering of the glass ceramics at lower temperatures. On the other hand, the glass phase can mitigate the formation of micro-cracks due to the thermal expansion anisotropy of the NaSICON phase [6,77], because it allows plastic deformation toward lower temperatures during cooling. This may not only increase the fracture toughness but also the ionic conductivity of such compounds.

4. Conclusions

For the series $Na_{3.4}Zr_{2-3x/4}Si_{2.4-x/4}P_{0.6+x/4}O_{12-11x/8}$ and $Na_{3.4}Zr_{2-3x/4}Si_{2.4+x/4}P_{0.6+1.5x/4}O_{12-x/16}$ with $0 < x < 0.8$, the applied methods gave clear evidence that a) the crystalline NaSICON phase show only a limited variation in composition and b) a vitreous phase is progressively formed with increasing x. Therefore, compounds with $x > 0.2$ have to be regarded as glass-ceramic composites. The Rietveld refinement of the ND patterns revealed a nearly constant Zr deficiency of 2–4%, which was confirmed by quantitative EDX analysis with slightly higher deficiencies (5–8%). Hence, the NaSICON materials equilibrated at high temperatures (1200–1250 °C) possess a limited Zr deficiency with charge compensation by the Na content and a non-detectable amount of oxygen vacancies. This charge compensation mechanism was also verified by the atomistic modeling. It also revealed an energetic benefit of the occupation of Zr vacancies with Na ions.

The correlation of the Na content with the melting points and the lattice constants gives first indications about the scatter of the compositions but is always based on the assumption that there are no Zr vacancies. The results of the ND and EDX analyses are much more reliable, and they additionally consistently suggest reduced Zr contents. Compositions with nominally high Zr deficiencies equilibrate in a rather narrow compositional regime that can be summarized as $Na_{3+z+4a}Zr_{2-a}Si_{2+z}P_{1-z}O_{12}$ with $0.1 < z < 0.4$ and $0.02 < a < 0.08$ (see Fig. 12).

In view of the results obtained here, the reports on the use of sintering aids (Na_2SiO_3 [46,47] and $Na_2Si_2O_5$ [48]) and substitution strategies [9,78] should be re-evaluated in a similar way, because additions of sodium silicates formally also create Zr deficiencies, exceeding the observed stability level (Table 3, Figs. 11c and 12).

CRediT authorship contribution statement

Enkhtsetseg Dashjav: Data curation, Formal analysis, Investigation, Validation, Writing – review & editing. **Marie-Theres Gerhards**: Data curation, Investigation. **Felix Klein**: Data curation, Formal analysis, Investigation, Writing – review & editing. **Daniel Grüner**: Data curation, Formal analysis, Investigation, Methodology, Writing – review & editing. **Thomas C. Hansen**: Data curation; Formal analysis, Investigation, Methodology. **Jochen Rohrer**: Data curation, Formal analysis, Investigation, Methodology, Software, Writing – review & editing. **Karsten Albe**: Data curation, Formal analysis, Funding acquisition, Investigation, Project administration, Software, Writing – review & editing. **Dina Fattakhova-Rohlfing**: Conceptualization, Formal analysis, Funding acquisition, Project administration, Supervision, Writing – review & editing. **Frank Tietz**: Conceptualization, Formal analysis, Funding acquisition, Project administration, Supervision, Visualization, Writing – original draft, Writing – review & editing

Declaration of Competing Interest

The authors declare the following financial interests/personal relationships which may be considered as potential competing interests: Frank Tietz reports financial support was provided by German Federal Ministry of Education and Research. Karsten Albe reports financial support was provided by German Federal Ministry of Education and Research. Dina Fattakhova-Rohlfing reports financial support was provided by Mercator Research Center Ruhr Foundation. If there are other authors, they declare that they have no known competing financial interests or personal relationships that could have appeared to influence the work reported in this paper.

Acknowledgments

Financial support from the German Federal Ministry of Education and Research (BMBF) within the project "HeNa" (support codes 13XP0390B and 13XP0390D) and the Mercator Research Center Ruhr Foundation (MERCUR) is gratefully acknowledged. The authors take responsibility for the content of this publication. The authors acknowledge the technical assistance of Mr. Volker Bader (IEK-1) for the heat treatments. The authors are also grateful for the provision of experimental facilities at ILL (Grenoble, France).

Supporting Information

Complementary data from this study are available in the supplement of this article. Crystallographic data files of this work are provided free of charge by the joint Cambridge Crystallographic Data Center and Fachinformationszentrum Karlsruhe, Access Structures service, and can be retrieved using the deposition numbers 2294186 (S1+2, $x = 0$), 2294170 (S1, $x = 0.2$), 2294185 (S1, $x = 0.4$), 2294189 (S1, $x = 0.6$), 2294209 (S1, $x = 0.8$), 2294143 (S2, $x = 0.2$), 2294169 (S2, $x = 0.4$), 2294283 (S2, $x = 0.8$).

Appendix A. Supporting information

Supplementary data associated with this article can be found in the online version at doi:10.1016/j.nxener.2024.100130.

References

[1] G.J. May, A. Hooper, The effect of microstructure and phase composition on the ionic conductivity of magnesium-doped sodium-beta-alumina, J. Mater. Sci. 13 (1978) 1480–1486, https://doi.org/10.1007/BF00553202.
[2] E. Yi, E. Temeche, R.M. Laine, Superionically conducting β''-Al_2O_3 thin films processed using flame synthesized nanopowders, J. Mater. Chem. A 6 (2018) 12411–12419, https://doi.org/10.1039/C8TA02907E.
[3] M.E. Brownfield, E. Foord, S.J. Sutley, T. Botinelly, Kosnarite, $KZr_2(PO_4)_3$, a new mineral from Mount Mica and Black Mountain, Oxford County, Maine, Am. Mineral. 78 (1993) 653–656.
[4] J.B. Goodenough, H.-Y.P. Hong, J. Kafalas, Fast Na^+-ion transport in skeleton structures, Mater. Res. Bull. 11 (1976) 203–220, https://doi.org/10.1016/0025-5408(76)90077-5.
[5] H.-Y.P. Hong, Crystal structures and crystal chemistry in the system $Na_{1+x}Zr_2Si_xP_{3-x}O_{12}$, Mater. Res. Bull. 11 (1976) 173–182, https://doi.org/10.1016/0025-5408(76)90073-8.
[6] F. Tietz, Sodium-ion-conducting oxides used as solid electrolytes in sodium batteries—learning from the past, in: M. Titirici, Ph Adelhelm, Y. Hu (Eds.), Sodium-Ion Batteries. Materials, Characterization, and Technology, Wiley-VCH, Weinheim, 2022, pp. 391–428.
[7] Q. Ma, C.-L. Tsai, X.K. Wei, M. Heggen, F. Tietz, J.T.S. Irvine, Room temperature demonstration of a sodium superionic conductor with grain conductivity in excess of 0.01 S cm^{-1} and its primary applications in symmetric battery cells, J. Mater. Chem. A 7 (2019) 7766–7776, https://doi.org/10.1039/C9TA00048H.
[8] Y. Noguchi, E. Kobayashi, Larisa S. Plashnitsa, S. Okada, J.-i Yamaki, Fabrication and performances of all solid-state symmetric sodium battery based on NASICON-related compounds, Electrochim. Acta 101 (2013) 59–65, https://doi.org/10.1016/j.electacta.2012.11.038.
[9] Z. Zhang, Q. Zhang, J. Shi, Y.S. Chu, X. Yu, K. Xu, M. Ge, H. Yan, W. Li, L. Gu, Y.-S. Hu, H. Li, X.-Q. Yang, L. Chen, X. Huang, A self-forming composite electrolyte for solid-state sodium battery with ultralong cycle life, Adv. Energy Mater. 7 (2017) 1601196, https://doi.org/10.1002/aenm.201601196.
[10] H. Gao, S. Xin, L. Xue, J.B. Goodenough, Stabilizing a high-energy-density rechargeable sodium battery with a solid electrolyte, Chemistry 4 (2018) 833–844, https://doi.org/10.1016/j.chempr.2018.01.007.
[11] T. Lan, C.-L. Tsai, F. Tietz, X.K. Wei, M. Heggen, R. Dunin-Borkowski, R. Wang, Y. Xiao, Q. Ma, O. Guillon, Room-temperature all-solid-state sodium batteries with robust ceramic interface between rigid electrolyte and electrode materials, Nano Energy 65 (2019) 104040, https://doi.org/10.1016/j.nanoen.2019.104040.
[12] H. Yamauchi, J. Ikejiri, F. Sato, H. Oshita, T. Honma, T. Komatsu, Pressureless all-solid-state sodium-ion battery consisting of sodium iron pyrophosphate glass-ceramic cathode and β''-alumina solid electrolyte composite, J. Am. Ceram. Soc. 102 (2019) 6658–6667, https://doi.org/10.1111/jace.16607.
[13] Y. Wang, Z. Wang, J. Sun, F. Zheng, M. Kotobuki, T. Wu, K. Zeng, L. Lu, Flexible, stable, fast-ion-conducting composite electrolyte composed of nanostructured Na-super-ion-conductor framework and continuous Poly(ethylene oxide) for all-solid-state Na battery, J. Power Sources 454 (2020) 227949, https://doi.org/10.1016/j.jpowsour.2020.227949.
[14] J.A.S. Oh, X. Xu, Z. Zeng, K. Wang, N.Y.J. Tan, E. Kok, J. Huang, L. Lu, Thin NASICON electrolyte to realize high energy density solid-state sodium metal battery, Energy Environ. Mater. 6 (2023) e12472, https://doi.org/10.1002/eem2.12472.
[15] J.M. Naranjo-Balseca, C.S. Martínez-Cisneros, B. Pandit, A. Várez, High performance NASICON ceramic electrolytes produced by tape-casting and low temperature hot-pressing: towards sustainable all-solid-state sodium batteries operating at room temperature, J. Eur. Ceram. Soc. 43 (2023) 4826–4836, https://doi.org/10.1016/j.jeurceramsoc.2023.04.008.
[16] P.W. Jaschin, C.R. Tang, E.D. Wachsman, High-rate cycling in 3D dual-doped NASICON architectures toward room-temperature sodium-metal-anode solid-state batteries, Energy Environ. Sci. 17 (2024) 727–737, https://doi.org/10.1039/d3ee03879c.
[17] A. Clearfield, R. Guerra, A. Oskarsson, M.A. Subramanian, W. Wang, Preparation of sodium zirconium phosphates of the type $Na_{1+4x}Zr_{2-x}(PO_4)_3$, Mater. Res. Bull. 18 (1983) 1561–1567, https://doi.org/10.1016/0025-5408(83)90198-8.
[18] A. Loutati, Y.J. Sohn, F. Tietz, Phase-field determination of NaSICON materials in the quaternary system $Na_2O-P_2O_5-SiO_2-ZrO_2$: the series $Na_3Zr_{3-x}Si_2P_xO_{11.5+x/2}$, ChemPhysChem 22 (2021) 995–1007, https://doi.org/10.1002/cphc.202100032.
[19] J.P. Boilot, G. Collin, R. Comès, Stoichiometry and phase transitions in NASICON type compounds, Solid State Ion. 9-10 (1983) 829–833, https://doi.org/10.1016/0167-2738(83)90097-8.
[20] U. von Alpen, M.F. Bell, H. Höfer, Compositional dependence of the electrochemical and structural parameters in the Nasicon system ($Na_{1+x}Si_xZr2P_{3-x}O_{12}$), Solid State Ion. 3-4 (1981) 215–218, https://doi.org/10.1016/0167-2738(81)90085-0.
[21] J. Engell, S. Mortensen, L. Møller, Fabrication of NASICON electrolytes from metal alkoxide derived gels, Solid State Ion. 9-10 (1983) 877–884, https://doi.org/10.1016/0167-2738(83)90105-4.
[22] S. Yde-Andersen, J.S. Lundgaard, L. Møller, J. Engell, Properties of nasicon electrolytes prepared from alkoxide derived gels: ionic conductivity, durability in molten sodium and strength test data, Solid State Ion. 14 (1984) 73–79, https://doi.org/10.1016/0167-2738(84)90014-6.
[23] A.K. Kuriakose, T.A. Wheat, A. Ahmad, J. Dirocco, Synthesis, sintering, and microstructure of NASICONs, J. Am. Ceram. Soc. 67 (1984) 179–183, https://doi.org/10.1111/j.1151-2916.1984.tb19737.x.
[24] H. Perthuis, Ph Colomban, Sol-gel routes leading to nasicon ceramics, Ceram. Int. 12 (1986) 39–52, https://doi.org/10.1016/S0272-8842(86)80008-6.
[25] W. Go, J. Kim, J. Pyo, J.B. Wolfenstine, Y. Kim, Investigation on the structure and properties of $Na_{3.1}Zr_{1.55}Si_{2.3}P_{0.7}O_{11}$ as a solid electrolyte and its application in a seawater battery, ACS Appl. Mater. Interfaces 13 (2021) 52727–52735, https://doi.org/10.1021/acsami.1c17338.
[26] F. Tietz, Phase relations of NASICON materials and compilation of the quaternary phase diagram $Na_2O-P_2O_5-SiO_2-ZrO_2$, AIMS Mater. Sci. 4 (2017) 1305–1318, https://doi.org/10.3934/matersci.2017.6.1305.
[27] M. Lucco-Borlera, D. Mazza, L. Montanaro, A. Negro, S. Ronchetti, X-ray characterization of the new nasicon compositions $Na3Zr_{2-x/4}Si_{2-x}P_{1+x}O_{12}$ with x = 0.333, 0.667, 1.000, 1.333, 1.667, Powder Differ. 12 (1997) 171–174, https://doi.org/10.1017/S0885715600009660.
[28] S. Naqash, Q. Ma, F. Tietz, O. Guillon, $Na_3Zr_2(SiO_4)_2(PO_4)$ prepared by a solution-assisted solid state reaction, Solid State Ion. 302 (2017) 83–91, https://doi.org/10.1016/j.ssi.2016.11.004.
[29] Q. Ma, M. Guin, S. Naqash, C.-L. Tsai, F. Tietz, O. Guillon, Scandium-substituted $Na_3Zr_2(SiO_4)_2(PO_4)$ prepared by a solution-assisted solid-state reaction method as sodium-ion conductors, Chem. Mater. 28 (2016) 4821–4828, https://doi.org/10.1021/acs.chemmater.6b02059.
[30] F. Liebau, Untersuchungen an Schichtsilikaten des Formeltyps $A_m(Si_2O_5)_n$. II. Über die Kristallstruktur des α-$Na_2Si_2O_5$, Acta Cryst. 14 (1961) 395–398, https://doi.org/10.1107/S0365110×61001315.
[31] A.K. Pant, D.W.J. Cruickshank, The crystal structure of α-$Na_2Si_2O_5$, Acta Cryst. B 24 (1968) 13–19, https://doi.org/10.1107/S0567740868001640.
[32] A. Grund, La structure cristalline du disilicate de soude β-$Na_2Si_2O_5$, Bull. Soc. franç. Min. éR. Crist. 77 (1954) 775–785.
[33] P. Porkodi, V. Yegnaraman, P. Kamaraj, V. Kalyanavalli, D. Jeyakumar, Synthesis of NASICON—a molecular precursor-based approach, Chem. Mater. 20 (2008) 6410–6419, https://doi.org/10.1021/cm800208k.
[34] V. Petricek, M. Dusek, L. Palatinus, Crystallographic computing system JANA2006: general features, Z. Krist. 229 (2014) 345–352, https://doi.org/10.1515/zkri-2014-1737.
[35] J. Rodriguez-Carvajal, Recent advances in magnetic structure determination by neutron powder diffraction, Physica B 192 (1993) 55–69, https://doi.org/10.1016/0921-4526(93)90108-I.
[36] J. Rodriguez-CarvajalJ. Rodriguez-Carvajal, Recent developments of the program FULLPROF, Commission on Powder Diffraction (IUCr), Newsletter 26, 2001, pp. 12-19.
[37] A.P. Thompson, H.M. Aktulga, R. Berger, D.S. Bolintineanu, W.M. Brown, P.S. Crozier, P.J. in't Veld, A. Kohlmeyer, S.G. Moore, T.D. Nguyen, R. Shan, M.J. Stevens, J. Tranchida, C. Trot, S.J. Plimpton, LAMMPS—a flexible simulation tool for particle-based materials modeling at the atomic, meso, and continuum scales, Comput. Phys. Commun. 271 (2022) 108171, https://doi.org/10.1016/j.cpc.2021.108171.
[38] J. Rohrer, K. Albe, manuscript in preparation.
[39] R. Drautz, Atomic cluster expansion for accurate and transferable interatomic potentials, Phys. Rev. B 99 (2019) 014104, https://doi.org/10.1103/PhysRevB.99.014104.

[40] A. Bochkarev, Y. Lysogorskiy, S. Menon, M. Qamar, M. Mrovec, R. Drautz, Efficient parametrization of the atomic cluster expansion, Phys. Rev. Mater. 6 (2022) 013804, https://doi.org/10.1103/PhysRevMaterials.6.013804.

[41] Y. Lysogorskiy, C. van der Oord, A. Bochkarev, S. Menon, M. Rinaldi, Th Hammerschmidt, M. Mrovec, A. Thompson, G. Csányi, Ch Ortner, R. Drautz, Performant implementation of the atomic cluster expansion (PACE) and application to copper and silicon, npj Comput. Mater. 7 (2021) 97, https://doi.org/10.1038/s41524-021-00559-9.

[42] J.J. Mortensen, L.B. Hansen, K.W. Jacobsen, Real-space grid implementation of the projector augmented wave method, Phys. Rev. B 71 (2005) 035109, https://doi.org/10.1103/PhysRevB.71.035109.

[43] J. Enkovaara, C. Rostgaard, J.J. Mortensen, J. Chen, M. Dułak, L. Ferrighi, J. Gavnholt, C. Glinsvad, V. Haikola, H.A. Hansen, Electronic structure calculations with GPAW: a real-space implementation of the projector augmented-wave method, J. Phys. 22 (2010) 253202, https://doi.org/10.1088/0953-8984/22/25/253202.

[44] K. Berland, P. Hyldgaard, Exchange functional that tests the robustness of the plasmon description of the van der Waals density functional, Phys. Rev. B 89 (2014) 035412, https://doi.org/10.1103/PhysRevB.89.035412.

[45] Ph Colomban, E. Mouchon, Phase transition in, thermal history and expansion of NASICON, solid solution and lithium derivative ceramics and of SiC (mullite) fibers-NASICON composites, Solid State Ion. 73 (1994) 209–220, https://doi.org/10.1016/0167-2738(94)90036-1.

[46] J.A.S. Oh, L. He, A. Plewa, M. Morita, Y. Zhao, T. Sakamoto, X. Song, W. Zhai, K. Zeng, L. Lu, Composite NASICON ($Na_3Zr_2Si_2PO_{12}$) solid-state electrolyte with enhanced Na^+ ionic conductivity: effect of liquid phase sintering, ACS Appl. Mater. Interfaces 11 (2019) 40125–40133, https://doi.org/10.1021/acsami.9b14986.

[47] H. Wang, G. Zhao, S. Wang, D. Liu, Z. Mei, Q. An, J. Jiang, H. Guo, Enhanced ionic conductivity of a $Na_3Zr_2Si_2PO_{12}$ solid electrolyte with Na_2SiO_3 obtained by liquid phase sintering for solid-state Na^+ batteries, Nanoscale 14 (2022) 823–832, https://doi.org/10.1039/D1NR06959D.

[48] B. Santhoshkumar, M.B. Choudhary, A.K. Bera, S.M. Yusuf, M. Ghosh, B. Pahari, High Na^+ conducting $Na_3Zr_2Si_2PO_{12}/Na_2Si_2O_5$ composites as solid electrolytes for Na^+ batteries, J. Am. Ceram. Soc. 105 (2022) 5011–5019, https://doi.org/10.1111/jace.18463.

[49] U. Warhus, Ph.D. thesis, University of Stuttgart, 1986.

[50] D. Tran Qui, J.J. Capponi, M. Gondrand, M. Saib, J.C. Joubert, R.D. Shannon, Thermal expansion of the framework in NASICON-type structure and its relation to Na^+ mobility, Solid State Ion. 3-4 (1981) 219–222.

[51] F. Tietz; E. Dashjav, T.C. Hansen; Phase analyses of Na ion-conducting glass-ceramic composites, 2023. Institut Laue-Langevin (ILL) doi:10.5291/ILL-DATA.5-22-807.

[52] J.P. Boilot, G. Collin, Ph Colomban, Crystal structure of the true nasicon: $Na_3Zr_2Si_2PO_{12}$, Mater. Res. Bull. 22 (1987) 669–676, https://doi.org/10.1016/0025-5408(87)90116-4.

[53] Z. Zhang, Z. Zou, K. Kaup, R. Xiao, S. Shi, M. Avdeev, Y.-S. Hu, D. Wang, B. He, H. Li, X. Huang, L.F. Nazar, L. Chen, Correlated migration invokes higher Na^+-Ion conductivity in NaSICON-type solid electrolytes, Adv. Energy Mater. 9 (2019) 1902373, https://doi.org/10.1002/aenm.201902373.

[54] P.R. Rudolf, M.A. Subramanian, A. Clearfield, J.D. Jorgensen, The crystal structure of a nonstoichiometric NASICON, Mater. Res. Bull. 20 (1985) 643–651, https://doi.org/10.1016/0025-5408(85)90142-4.

[55] E.-T. Kang, H. Cheong, J.-S. Choi, J.-B. Choi, Crystal structure of NASICON by rietveld structural refinement, Korean J. Mater. Res. 6 (1996) 504–514.

[56] P.R. Rudolf, A. Clearfield, J.D. Jorgensen, Rietveld refinement results on three nonstoichiometric monoclinic NASICONs, Solid State Ion. 21 (1986) 213–224, https://doi.org/10.1016/0167-2738(86)90075-5.

[57] E.A. Cheung, H. Nguyen, M. Avdeev, N.R. De Souza, Y.S. Meng, N. Sharma, Insights into the fast sodium conductor NASICON and the effects of Mg^{2+} doping on Na^+ conductivity, Chem. Mater. 33 (2021) 8768–8774, https://doi.org/10.1021/acs.chemmater.1c02846.

[58] E. Heo, J.E. Wang, J.H. Yun, J.-H. Kim, D.J. Kim, D.K. Kim, Inorg. Chem. 60 (2021) 11147.

[59] W.H. Baur, J.R. Dygas, D.H. Whitmore, J. Faber, Neutron powder diffraction study and ionic conductivity of $Na_2Zr_2SiP_2O_{12}$ and $Na_3Zr_2Si_2PO_{12}$, Solid State Ion. 18-19 (1986) 935–943.

[60] H. Park, K. Jung, M. Nezafati, C.-S. Kim, B. Kang, Sodium Ion diffusion in NASICON ($Na_3Zr_2Si_2PO_{12}$) solid electrolytes: effects of excess sodium, ACS Appl. Mater. Interfaces 8 (2016) 27814–27824, https://doi.org/10.1021/acsami.6b09992.

[61] R.D. Shannon, Revised effective ionic radii and systematic studies of interatomie distances in halides and chaleogenides, Acta Cryst. A 32 (1976) 751–767, https://doi.org/10.1107/S0567739476001551.

[62] U. von Alpen, M.F. Bell, H. Höfer, Ionic conductivity in $Na_4ZrSi_3O_{10}$, Solid State Ion. 7 (1982) 345–348.

[63] H. Perthuis, Ph Colomban, Well densified nasicon type ceramics, elaborated using sol-gel process and sintering at low temperatures, Mater. Res. Bull. 19 (1984) 621–631, https://doi.org/10.1016/0025-5408(84)90130-2.

[64] S. Susman, C.J. Delbecq, J.A. McMillan, M.F. Roche, NASIGLAS: a new vitreous electrolyte, Solid State Ion. 9-10 (1983) 667–673.

[65] A. Niyompan, D. Holland, NASIGLAS structure and properties, J. Non-Cryst. Solids 293-295 (2001) 709–714, https://doi.org/10.1016/S0022-3093(01)00781-5.

[66] H. Kohler, H. Schulz, O. Melnikov, Composition and conduction mechanism of the NASICON structure X-ray diffraction study on two crystals at different temperatures, Mater. Res. Bull. 18 (1983) 1143–1152, https://doi.org/10.1016/0025-5408(83)90158-7.

[67] H. Kohler, H. Schulz, Single crystal investigations on NASICON Na/1 + z/Zr/2 − y/Si/x/P/3 − x/0/12/; $0 \leq y \leq 3/4$, $0 \leq z \leq 0$ comparison of the compounds $x = 1.24$ and $x = 3$, Solid State Ion. 9-10 (1983) 795–798.

[68] H. Kohler, H. Schulz, O. Melnikov, Structural investigations of NASICON ($Na_{1+x}Zr_2Si_xP_{3-x}O_{12}$; $x = 3$) with x-ray diffraction at 298K and 403K, Mater. Res. Bull. 18 (1983) 589–592, https://doi.org/10.1016/0025-5408(83)90216-7.

[69] E. Traversa, H. Aono, Y. Sadaoka, L. Montanaro, Electrical properties of sol–gel processed NASICON having new compositions, Sens. Actuators B 65 (2000) 204–208, https://doi.org/10.1016/S0925-4005(99)00293-2.

[70] J.P. Boilot, G. Collin, R. Comès, Zirconium deficiency in nasicon-type compounds: crystal structure of $Na_5Zr(PO_4)_3$, J. Solid State Chem. 50 (1983) 91–99, https://doi.org/10.1016/0022-4596(83)90236-0.

[71] J.P. Boilot, G. Collin, R. Comès, Evidence of a relation between structural defects and phase transitions in NASICON type compounds, Solid State Commun. 45 (1983) 231–236, https://doi.org/10.1016/0038-1098(83)90470-2.

[72] J.P. Boilot, G. Collin, Ph Colomban, Relation structure-fast ion conduction in the NASICON solid solution, J. Solid State Chem. 73 (1988) 160–171, https://doi.org/10.1016/0022-4596(88)90065-5.

[73] A.H. Larsen, J.J. Mortensen, J. Blomqvist, I.E. Castelli, R. Christensen, M. Dułak, J. Friis, M.N. Groves, B. Hammer, C. Hargus, E.D. Hermes, P.C. Jennings, P.B. Jensen, J. Kermode, J.R. Kitchin, E.L. Kolsbjerg, J. Kubal, K. Kaasbjerg, S. Lysgaard, J. Bergmann Maronsson, T. Maxson, T. Olsen, L. Pastewka, A. Peterson, C. Rostgaard, J. Schiøtz, O. Schütt, M. Strange, K.S. Thygesen, T. Vegge, L. Vilhelmsen, M. Walter, Z. Zeng, K.W. Jacobsen, The atomic simulation environment—a Python library for working with atoms, J. Phys. 29 (2017) 273002, https://doi.org/10.1088/1361-648X/aa680e.

[74] F. Tietz, J. Koepke, W. Urland, Analytical investigations of β-Al_2O_3 and β''-Al_2O_3 crystals, J. Cryst. Growth 118 (1992) 314–318, https://doi.org/10.1016/0022-0248(92)90078-W.

[75] E.T. Turkdogan, W.R. Maddocks, Phase equilibrium investigation of the Na_2O-P_2O_5-SiO_2 ternary system, J. Iron Steel Inst. 172 (1952) 1–15.

[76] T.O. Mason, F.A. Hummel, Compatibility relations in the system SiO_2-ZrO_2-P_2O_5, J. Am. Ceram. Soc. 57 (1974) 538–539.

[77] J. Alamo, R. Roy, Commun. Ultralow-expansion ceramics in the system Na_2O-ZrO_2-P_2O_5-SiO_2, Am. Ceram. Soc. 67 (1984) C78–C80, https://doi.org/10.1111/j.1151-2916.1984.tb19516.x.

[78] I.-S. Jang, W. Go, B.-Y. Song, H. Park, Y.C. Kang, J. Chun, Improving ionic conductivity of von-Alpen-type NASICON ceramic electrolytes via magnesium doping, J. Adv. Ceram. 12 (2023) 1058–1066, https://doi.org/10.26599/JAC.2023.9220738.